B CELLS

RNA exosome drives early B cell development via noncoding RNA processing mechanisms

Brice Laffleur[1]*†‡, Carolina R. Batista[1]‡, Wanwei Zhang[1]‡, Junghyun Lim[1], Biao Yang[1], Delphine Rossille[2]†, Lijing Wu[1], Jerson Estrella[1], Gerson Rothschild[1], Evangelos Pefanis[3], Uttiya Basu[1]*§

B cell development is linked to successful V(D)J recombination, allowing B cell receptor expression and ultimately antibody secretion for adaptive immunity. Germline noncoding RNAs (ncRNAs) are produced at immunoglobulin (Ig) loci during V(D)J recombination, but their function and posttranscriptional regulation are incompletely understood. Patients with trichohepatoenteric syndrome, characterized by RNA exosome pathway component mutations, exhibit lymphopenia, thus demonstrating the importance of ncRNA surveillance in B cell development in humans. To understand the role of RNA exosome in early B cell development in greater detail, we generated mouse models harboring a B cell–specific *cre* allele (*Mb1^{cre}*), coupled to conditional inversion-deletion alleles of one RNA exosome core component (*Exosc3*) or RNase catalytic subunits (*Exosc10* or *Dis3*). We noticed increased expression of RNA exosome subunits during V(D)J recombination, whereas a B cell developmental blockade at the pro–B cell stage was observed in the different knockout mice, overlapping with a lack of productive rearrangements of VDJ genes at the *Ig* heavy chain (*Igh*). This unsuccessful recombination prevented differentiation into pre–B cells, with accumulation of ncRNAs and up-regulation of the p53 pathway. Introduction of a prearranged *Igh* VDJ allele partly rescued the pre–B cell population in *Dis3*-deficient cells, although V-J recombination defects were observed at *Ig* light chain kappa (*Igκ*), preventing subsequent B cell development. These observations demonstrated that the RNA exosome complex is important for *Igh* and *Igκ* recombination and establish the relevance of RNA processing for optimal diversification at these loci during B cell development.

INTRODUCTION

Adaptive immunity relies on the generation of new antigen receptors in T and B lymphocytes through V(D)J recombination, an antigen-independent recombination between variable (V), diversity (D), and joining (J) gene segments in the immunoglobulin (Ig) locus. Pro–B cells undergo D to J_H, followed by V_H to DJ_H recombination of their Ig heavy chain (*Igh*), inducing the expression of a precursor B cell receptor (pre-BCR) that provides survival and proliferation signals and allows light chain rearrangement (*1*). In the Ig light chain loci (IgL), either Igκ or Igλ, recombination occurs in pre–B cells between V_L and J_L genes, inducing membrane expression of a functional BCR, intracellular signaling, cell differentiation, and exit from the bone marrow and circulation in the periphery (*2*). These processes of gene rearrangement and cellular differentiation occur in distinct stages during B cell development and are critical to ensure a diverse B cell repertoire and high-affinity antibody production.

Multiple mechanisms stringently regulate V(D)J recombination, including temporal and developmental stage–specific expression of the recombinases *Rag1* and *Rag2* (recombination-activating genes), Ig gene positioning, chromosome organization, and open chromatin state (*3*). Ig genes undergo epigenetic changes before V(D)J recombination, including DNA demethylation, histone modification, and variations in deoxyribonuclease hypersensitivity. These changes open the chromatin to permit the RAG proteins access to the recombination signal sequences (RSSs) (*4*). RAG is an evolutionarily conserved endonuclease that binds and cuts double-strand DNA. RAG structure (*5*) and mode of action (*6*) suggest that noncoding transcription could impede its DNA binding properties and cleavage activity if noncoding RNAs (ncRNAs) overlap RSS sites. Germline sense and antisense noncoding transcription is observed at different elements of *Ig* loci (*7*–*9*). ncRNA processing and RNA surveillance also control loop extrusion mechanisms (*10*) implicated in RAG1/2 accessibility during V(D)J recombination (*11*–*13*). Last, RAG1 protein is negatively regulated via sequestration in the nucleolus, and accumulated nucleolar ncRNA could inhibit RAG1's Ig recombinational activity (*14*). Together, RNA surveillance of ncRNA could influence V(D)J recombination via multiple mechanisms.

RNA surveillance and noncoding decay are mediated by the RNA exosome, a multiprotein complex with 3′ to 5′ ribonuclease activity implicated in the processing and decay of various classes of RNAs in the nucleus (*15*) and DNA or chromatin-associated RNAs (*10*, *16*, *17*). The eukaryotic RNA exosome is composed of a catalytically inactive, nine essential subunit core that associates with 3′ to 5′ ribonucleases DIS3 and EXOSC10 in humans. Multiple myeloma (*18*, *19*) and immunodeficiencies such as trichohepatoenteric syndrome (THES) syndrome (*20*) have been associated with mutations in RNA surveillance genes, such as *DIS3* and *SKIV2L* in humans, respectively, although their precise contributions in disease development remain to be elucidated.

The RNA exosome plays a fundamental role in degrading germline transcripts at repetitive and G-rich switch regions [necessary for class switch recombination (CSR)] during B cell activation, providing DNA accessibility to activation-induced deaminase (AID) for

[1]Department of Microbiology and Immunology, Vagelos College of Physicians and Surgeons, Columbia University, New York, NY 10032, USA. [2]Universite of Rennes, INSERM, EFS Bretagne, CHU Rennes, UMR 1236, Rennes, France. [3]Regeneron Pharmaceuticals, Tarrytown, New York, NY 10591, USA.
*Corresponding author. Email: laffleur.brice@gmail.com (B.L.); ub2121@cumc.columbia.edu (U.B.)
†Present address: Université of Rennes, INSERM, Etablissement Français du Sang Bretagne, UMR 1236, Rennes, France.
‡These authors contributed equally to this work.
§Lead contact.

optimal CSR (*10*, *21*, *22*). Here, we demonstrated that RNA exosome subunits were highly expressed during stages of antigen receptor loci diversification [both V(D)J recombination and CSR]. The RNA exosome was required for B cell development from the pro–B cell to the pre–B cell stages and mediated processing of germline transcripts needed for V(D)J recombination.

Lack of RNA exosome activity led to defects during *Igh* locus recombination, impeding pre-BCR signaling and consequently blocking B cell development at the pro–B cell stage. Failure of proper pre-BCR signaling in pro–B cells ultimately led to the activation of the p53 pathway. *Igk* locus recombination defects were also observed, suggesting that RNA exosome also contributed to the generation of VJ gene rearrangements and BCR expression in pre–B cells. Together, our study provides evidence that RNA exosome–mediated surveillance of noncoding transcripts is important during early B cell development.

RESULTS

Expression of RNA exosome subunits during early B cell development

B cell development is initiated in the bone marrow where V(D)J genes undergo DNA recombination (*3*). Subsequent encounter with antigen triggers another round of *Ig* gene diversification by somatic hypermutation (SHM) and CSR during the germinal center (GC) reaction (*23*). Developing B cell populations are characterized by specific transcriptomic programs, which control the expression of the RAG recombinases and AID to initiate recombination. We asked whether expression of the RNA exosome subunits changes during early B cell development in the bone marrow by analyzing publicly available transcriptomic data from the Immunological Genome Project (ImmGen). RNA exosome subunits were expressed in all developing B cell subpopulations; however, we observed a higher expression of certain subunits including *Exosc3*, *Exosc10*, and *Dis3* in GC B cells (Fig. 1A). Higher expression levels in GC cells correlated with already described crucial functions of RNA exosome in CSR and SHM processes (*10*, *24*, *25*). In parallel, we also observed

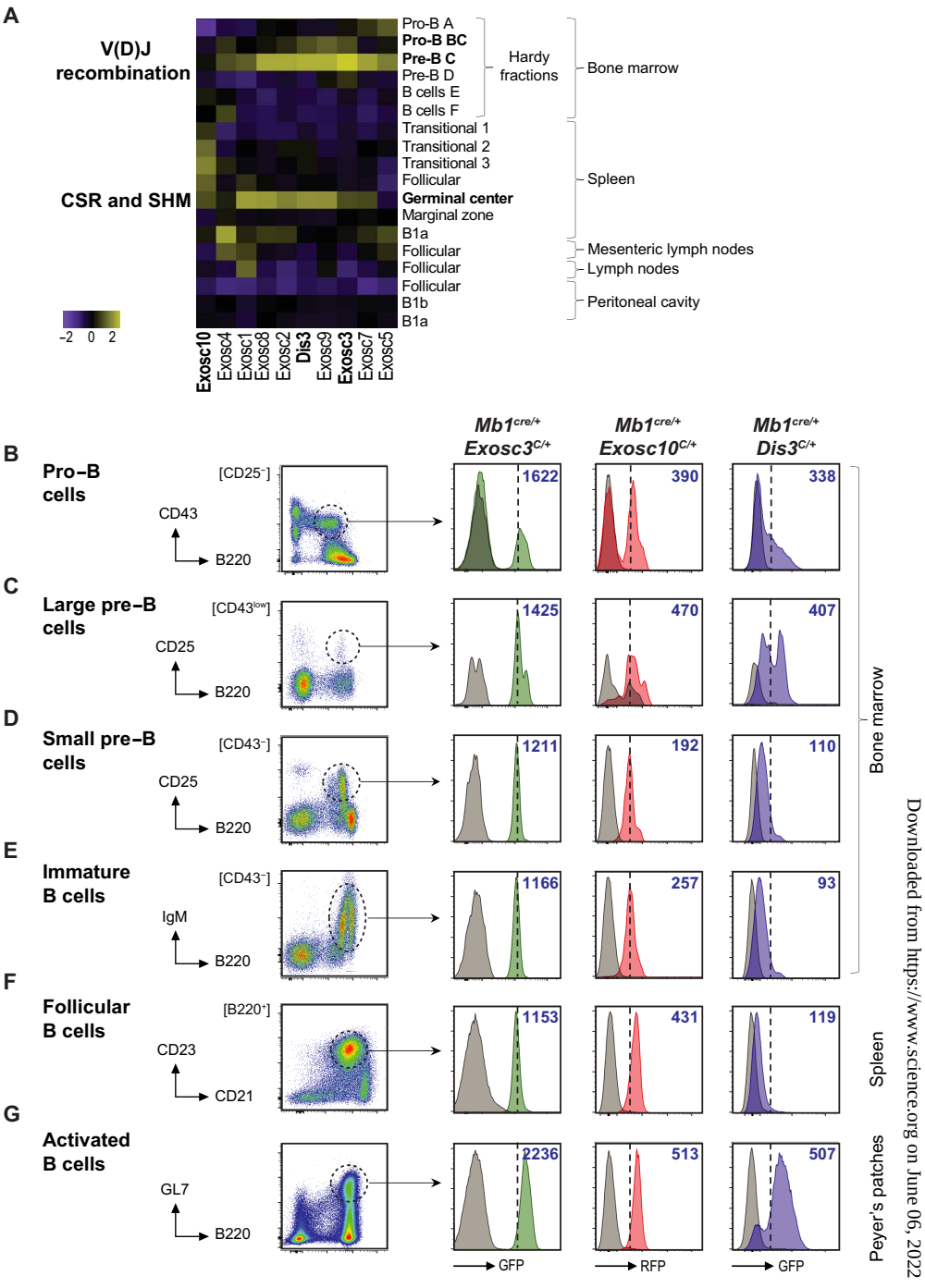

Fig. 1. Dynamic RNA exosome subunits expression during B cell development. (**A**) Heatmap showing RNA exosome subunit expression in mouse B cells; data were obtained from "ImmGen" databank. Relative transcriptomic expression of the RNA exosome subunits is shown in the main B cell populations from various lymphoid organs in adult mice. (**B** to **G**) Flow cytometry analysis of *Mb1*$^{cre/+}$ *Exosc3*$^{COIN/+}$, *Mb1*$^{cre/+}$ *Exosc10*$^{COIN/+}$, and *Mb1*$^{cre/+}$ *Dis3*$^{COIN/+}$ B cell populations. Cells were collected from the bone marrow, spleen, and Peyer's patches, and the B cell populations were identified as (B) pro–B cells (CD43^{+}, B220^{+}, CD25$^{−}$, and IgM$^{−}$), (C) large pre–B cells (FSC-A^{high}, CD43^{low}, B220^{+}, and CD25^{low}), (D) small pre–B cells (CD43$^{−}$, B220^{+}, CD25^{+}, and IgM$^{−}$), (E) immature B cells (CD43$^{−}$, B220^{+}, CD25$^{−}$, and IgM^{+}), (F) follicular B cells (B220^{+}, CD23^{+}, and CD21^{dim}), and (G) activated B cells (B220^{+} and GL7^{+}). GFP or RFP expression is shown in each subpopulation after specific gating. *Mb1*$^{cre/+}$ mice were used as control for GFP/RFP expression, shown as gray histograms. The dashed line represents the threshold for high GFP/RFP expression. Mean fluorescent intensities of GFP^{+}/RFP^{+} cells are indicated in blue (see also fig. S1, F to H). These data are representative from at least three independent experiments per genotype, using a total of at least three mice per group.

higher expression of most RNA exosome subunits in pro–/pre–B cells (Hardy fractions B and C; note that Hardy fractions define B cell precursors into subpopulations based on cell surface marker expression), found during V(D)J recombination both in the adult bone marrow (postnatal immune system; Fig. 1A) and in the fetal liver (prenatal immune system; fig. S1A). To investigate the importance of these observations in vivo, we developed dedicated mouse models to delete RNA exosome components in early B cell development using $Mb1^{cre}$ mice (*26*) in combination with *COIN* alleles for *Exosc3* (RNA exosome core subunit), *Exosc10*, or *Dis3* (RNA exosome catalytic subunits; fig. S1, B to D) (*10*, *24*, *25*). *COIN* heterozygous mice served as the reporter system; in these mice, one allele remains functional, whereas green fluorescent protein (GFP)/red fluorescent protein (RFP) expression from the other allele depends on endogenous *Exosc3*, *Exosc10*, or *Dis3* promoters after *cre*-mediated inversion of the *COIN* allele (fig. S1, B to D). We found that heterozygous mice lacked a notable phenotype, as shown by the percentage of B splenocytes in $Mb1^{cre/+}$ $Dis3^{C/+}$ compared with $Mb1^{cre/+}$ $Dis3^{+/+}$ mice (fig. S1E). To confirm the expression of the RNA subunits *Exosc3*, *Exosc10*, and *Dis3* in B cell subsets present in the bone marrow, spleen, and Peyer's patches, we performed flow cytometry using a combination of known B cell development markers. We compared the levels of GFP/RFP expression, which are driven by *Exosc3*, *Exosc10*, and *Dis3* gene promoters, as a readout for the expression of RNA exosome subunits in these cells. As expected, GFP/RFP reporter gene expression was noted at the pro–B cell stage in the bone marrow, when *cre* recombinase was expressed and *COIN* alleles were inverted (Fig. 1B). Developing pre–B cells and immature B cells continued to express GFP/RFP proteins in the bone marrow (Fig. 1, C to E) before exiting to the periphery. Follicular B splenocytes were GFP/RFP-positive, and activated B cells from Peyer's patches also expressed *Exosc3*, *Exosc10*, and *Dis3* (Fig. 1, F and G). Consistent with transcriptomic data, we detected increased expression of *Exosc3*, *Exosc10*, and *Dis3* specifically in bone marrow–developing pro–B cells and large pre–B cells during V(D)J recombination and in activated B cells (Fig. 1, B, C, and G; and fig. S1, F to H). We noted a distinct expression pattern for *Exosc10* that was also expressed during the transitional stages (Fig. 1A) and in follicular B cells in the spleen (Fig. 1, A and F, and fig. S1G; please see fig. S2A for schematic of B cell development). Expression of genes encoding RNA exosome subunits was observed in other cell types in a random manner, contrasting with the expression trend noted in B cells (fig. S2, B to D). We also observed higher expression of other components of the RNA surveillance machinery, such as the RNA helicases *Ddx1*, *Ddx19a*, *Ddx41*, and *Skiv2l* during early B cell development and in activated GC B cells (fig. S2E). Last, motif enrichment analysis revealed common transcription factor (such as *Spi1*, *Spib*, and others) binding sites located ~250–base pair upstream of the ATG sequences of *Exosc3*, *Exosc10*, and *Dis3* gene promoters explaining a similar coregulation and coexpression profile observed in B cells (fig. S2F). Thus, our results suggest that RNA exosome subunit and cofactor expression can be temporally regulated during B cell development in vivo and are notably increased during B cell developmental stages that are associated with antigen receptor gene diversification.

The RNA exosome supports the pro–B cell to pre–B cell transition and *Igh* rearrangement

To evaluate the contribution of RNA exosome activity during B cell development, we used three B cell–specific conditional knockout mouse models harboring homozygous *COIN* alleles ($Exosc3^{COIN}$, $Exosc10^{COIN}$, and $Dis3^{COIN}$). Flow cytometry analyses indicated that bone marrow–developing B cells were blocked at the pro–B cell stage, whereas B cells were poorly able to differentiate into pre–B cells in the absence of *Exosc3*, *Exosc10*, and *Dis3* (Fig. 2, A and B). Bone marrow small pre–B cells and immature B cells consequently were decreased greatly (Fig. 2, C and D). Loss of RNA exosome subunits that led to the accumulation of pro–B cells in the bone marrow could be caused by an inability of pro–B cells to rearrange *Igh* genes. *Igh* polymerase chain reaction (PCR) assays detected a slight decrease in D to J_H recombination (fig. S3A), whereas V_H to DJ_H recombination was greatly decreased at V_HJ558 distal or V_H7183 proximal genes in the absence of the RNA exosome (fig. S3, B to D).

To perform an accurate and unbiased quantification of the V(D)J recombination events in these cells, we sorted bone marrow pro–B cells and performed deep RNA sequencing (RNA-seq) analysis. We reconstituted the Ig VDJ sequences from RNA-seq data (using computational tool TRUST4) and performed a V-quest analysis using the international ImMunoGeneTics information system (IMGT) database. These analyses reconstituted the unique VDJ rearrangements from the RNA-seq data, and we normalized these unique rearrangements to the total number of reads. We were able to reconstitute 7482 functional VDJ junctions of 648,140,008 reads in controls (11.55 per million reads) versus 1326 functional VDJ junctions of 671,548,696 reads (1.98 per million reads) in DIS3-deficient pro–B cells, demonstrating a defect in VDJ recombination in the absence of the RNA exosome, affecting the frequencies of both V_H and J_H gene usage (Fig. 2, E and F). By focusing on the productive rearrangements, the percentages/distribution of the different V_H family was not altered (fig. S3E). Chromatin regulation is associated with RNA exosome activity and RNA exosome–sensitive ncRNAs (*25*, *27*). However, chromatin accessibility in the *Igh* locus, as measured by assay for transposase-accessible chromatin with high-throughput sequencing (ATAC-seq) in sorted pro–B cells ($B220^+$ $CD43^+$ IgM^-), remained unchanged (fig. S3, F and G), suggesting that this defect is not due to a lack of open chromatin but rather to the accumulation of noncoding transcripts in the absence of DIS3. Repertoire analyses revealed a decrease in CDR3 length in cells lacking ribonuclease activity, suggesting that RNA processing is necessary for accurate VDJ junctions (Fig. 2G). Together, our findings highlight a role for RNA exosome in early B cell development via mechanisms that involve antigen receptor locus recombination.

B cell development is affected by the deletion of RNA exosome subunits

Despite the strong block in B cell development at the pro–B cell stage, a small percentage of B cells were able to exit the bone marrow and migrate into the periphery, populating the spleen and Peyer's patches. Flow cytometry analyses showed that follicular B cells were substantially affected by the absence of the RNA exosome subunits (Fig. 3, A and B). In contrast, the percentages of marginal zone (MZ) B cells were not significantly decreased (Fig. 3, A and C). This leads to higher MZ/follicular B cell ratios in the absence of RNA exosome activity (Fig. 3D). In the gut-associated lymphoid tissue Peyer's patches, both resting and activated B cells were decreased in the absence of the RNA exosome catalytic subunits (Fig. 3, E to G). We also compared RNA exosome–proficient versus RNA exosome–deficient mice by combining all the RNA exosome–deficient

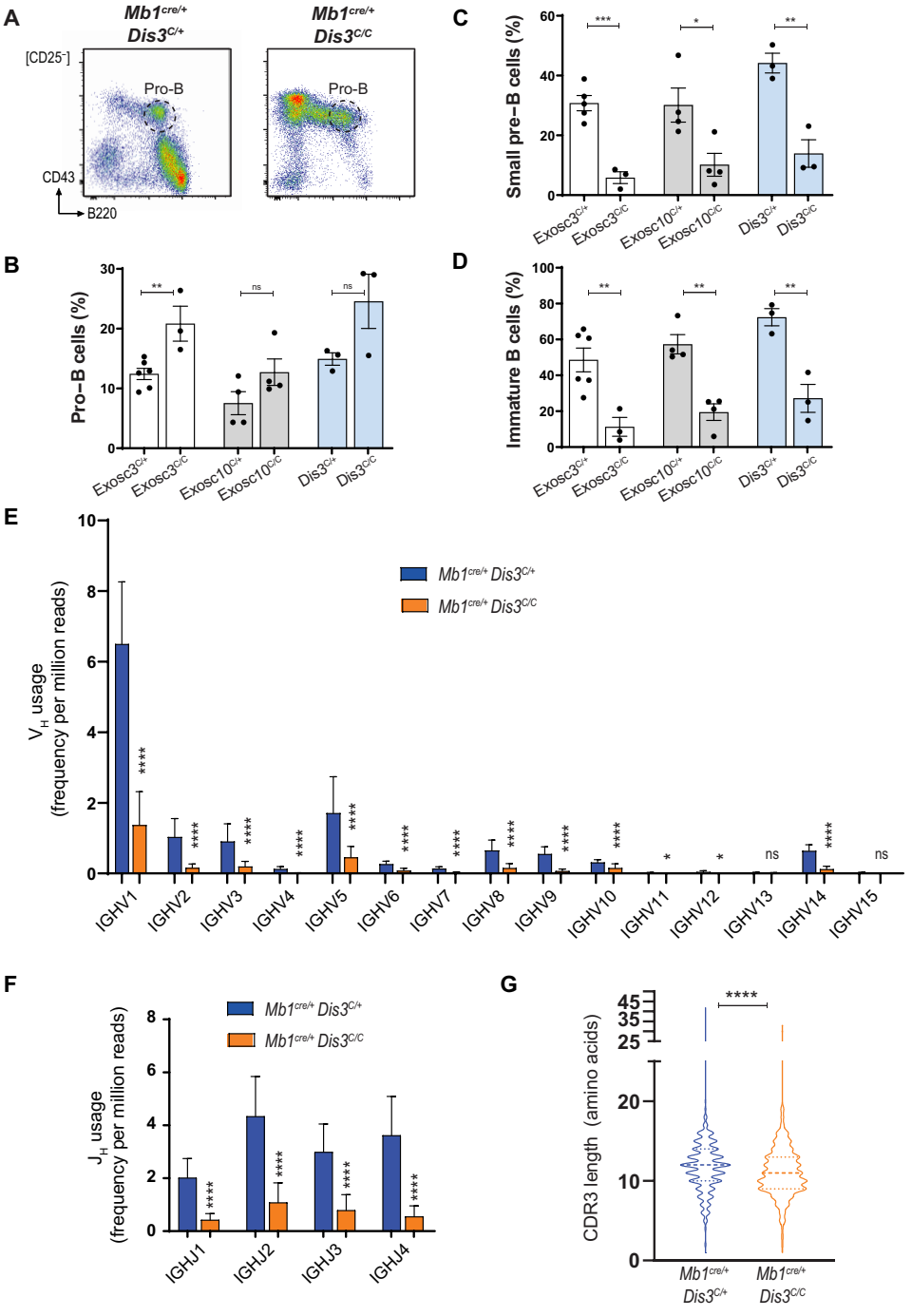

Fig. 2. RNA exosome is mandatory for early B cell development and *Igh* recombination. (**A**) Flow cytometry analysis of bone marrow pro–B cell populations from *Mb1*$^{cre/+}$ *Dis3*$^{C/+}$ and *Mb1*$^{cre/+}$ *Dis3*$^{C/C}$ mice. (**B**) Quantification of bone marrow pro–B cells (CD43$^+$, B220$^+$, CD25$^-$, and IgM$^-$), from *Mb1*$^{cre/+}$ *Exosc3*$^{C/+}$, *Mb1*$^{cre/+}$ *Exosc3*$^{C/C}$, *Mb1*$^{cre/+}$ *Exosc10*$^{C/+}$, *Mb1*$^{cre/+}$ *Exosc10*$^{C/C}$, *Mb1*$^{cre/+}$ *Dis3*$^{C/+}$, and *Mb1*$^{cre/+}$ *Dis3*$^{C/C}$ mice. (**C**) Quantification of bone marrow small pre–B cells (CD43$^-$, B220$^+$, CD25$^+$, and IgM$^-$). (**D**) Quantification of bone marrow immature B cells (CD43$^-$, B220$^+$, CD25$^-$, and IgM$^+$). These results are representative from at least three independent experiments, using a total of at least three mice per group. Bar graphs show mean value ± SEM, analyzed with two-tailed unpaired *t* test. (**E**) V_H repertoire in *Mb1*$^{cre/+}$ *Dis3*$^{C/+}$ and *Mb1*$^{cre/+}$ *Dis3*$^{C/C}$ pro–B cells. Mean is shown, ±SEM. (**F**) J_H repertoire in *Mb1*$^{cre/+}$ *Dis3*$^{C/+}$ and *Mb1*$^{cre/+}$ *Dis3*$^{C/C}$ pro–B cells. Mean is shown, ±SEM. The VDJ repertoire was determined by RNA-seq of pro–B cells (three independent experiments), and the number of productive V(D)J rearrangements compared with the total number of reads was used to perform statistical analyses (Khi2 proportion test). (**G**) CDR3 length was analyzed, and the violin plots show their distribution in the presence or absence of DIS3 (two-tailed unpaired *t* test on combined data from three mice). *P < 0.05; **P < 0.01; ***P < 0.001; ****P < 0.0001.

genotypes (*Exosc3*, *Dis3*, and *Exosc10*) and confirmed the accumulation of pro–B cells and the consequent decrease in other B cell subsets. In addition, we noted an altered MZ/follicular B cell ratio (fig. S4, A to C). Further independent experiments confirmed the altered MZ/follicular B cell ratio in the absence of *Dis3* (fig. S4, D and E). Collectively, these data suggest that the functionality of RNA exosome degradation machinery is not restricted to the early developmental stages where B cell precursors are recombining their *Ig* genes. RNA exosome activity potentially is required for regulating the expression levels of genes controlling fate decision, as B cells enter the follicles or the MZ in the secondary lymphoid organs.

Dis3 deletion leads to an accumulation of noncoding transcripts and up-regulation of the p53 pathway

To determine whether ncRNA accumulation could occur during defective B cell development in RNA exosome–deficient B cells, we investigated the transcriptome of *Mb1*$^{cre/+}$ *Dis3*$^{C/C}$ pro–B cells. The transcriptome from RNA exosome–deficient cells is a robust tool for detecting transiently expressed ncRNAs that are normally expressed but difficult to detect in RNA exosome–proficient cells (*10*, *24*, *25*). We validated efficient depletion of *Dis3* mRNA in vivo in homozygous cells (fig. S5A) and analyzed DIS3-sensitive RNA substrates. In bone marrow–derived developing pro–B cells, long ncRNAs (lncRNAs; Fig. 4A), intergenic and intragenic enhancer-associated RNAs (eRNAs; Fig. 4B), and antisense transcription start site at promoters (aTSS-RNAs; Fig. 4C) have altered expression and were perturbed genome wide (Fig. 4D). We also confirmed accumulation of antisense RNAs (asRNAs), whereas mRNA levels were not pervasively perturbed (Fig. 4D), consistent with our previous observations in activated B cells (*10*, *24*, *25*). We showed multiple examples of ncRNAs, including aTSS-RNAs, asRNAs in gene bodies (fig. S5, B and C), and eRNAs (fig. S5D) that were sensitive to DIS3 activity. RNA exosome deficiency did not reduce the expression of pro–B cell essential genes, such as *Irf4*, *Il7r*, or the *Rag1/2* recombinases (fig. S5, B, C, and E), whereas ncRNAs consistently accumulated at different regions of the genome (fig. S5F).

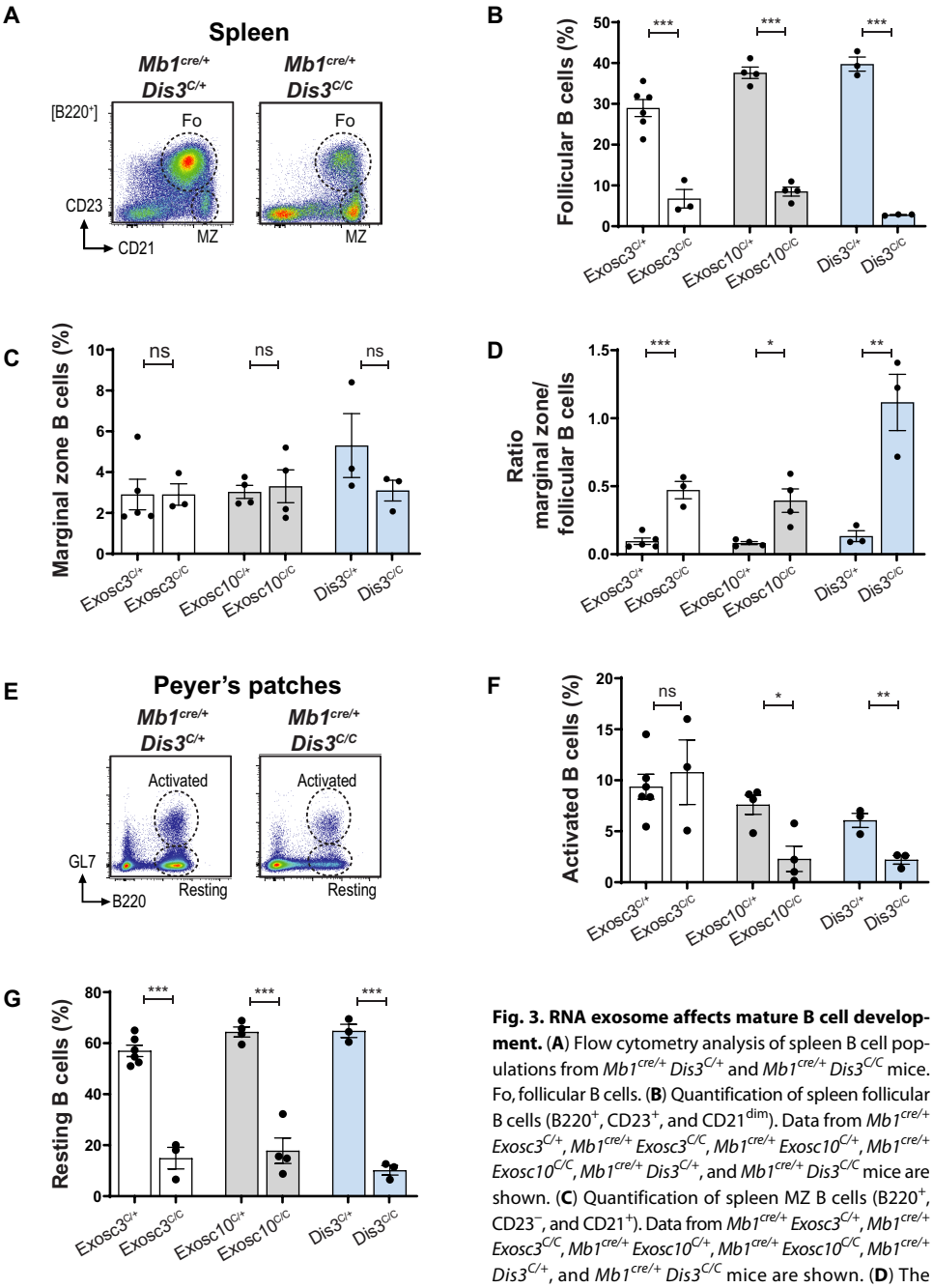

Fig. 3. RNA exosome affects mature B cell development. (**A**) Flow cytometry analysis of spleen B cell populations from *Mb1*$^{cre/+}$ *Dis3*$^{C/+}$ and *Mb1*$^{cre/+}$ *Dis3*$^{C/C}$ mice. Fo, follicular B cells. (**B**) Quantification of spleen follicular B cells (B220^{+}, CD23^{+}, and CD21^{dim}). Data from *Mb1*$^{cre/+}$ *Exosc3*$^{C/+}$, *Mb1*$^{cre/+}$ *Exosc3*$^{C/C}$, *Mb1*$^{cre/+}$ *Exosc10*$^{C/+}$, *Mb1*$^{cre/+}$ *Exosc10*$^{C/C}$, *Mb1*$^{cre/+}$ *Dis3*$^{C/+}$, and *Mb1*$^{cre/+}$ *Dis3*$^{C/C}$ mice are shown. (**C**) Quantification of spleen MZ B cells (B220^{+}, CD23^{-}, and CD21^{+}). Data from *Mb1*$^{cre/+}$ *Exosc3*$^{C/+}$, *Mb1*$^{cre/+}$ *Exosc3*$^{C/C}$, *Mb1*$^{cre/+}$ *Exosc10*$^{C/+}$, *Mb1*$^{cre/+}$ *Exosc10*$^{C/C}$, *Mb1*$^{cre/+}$ *Dis3*$^{C/+}$, and *Mb1*$^{cre/+}$ *Dis3*$^{C/C}$ mice are shown. (**D**) The ratios of MZ/follicular B cells (C and D) were quantified from these mice. (**E**) Flow cytometry analysis of Peyer's patches B cell populations from *Mb1*$^{cre/+}$ *Dis3*$^{C/+}$ and *Mb1*$^{cre/+}$ *Dis3*$^{C/C}$ mice. (**F**) Quantification of Peyer's patches resting B cells (B220^{+} GL7^{-}). Data were obtained from *Mb1*$^{cre/+}$ *Exosc10*$^{C/+}$, *Mb1*$^{cre/+}$ *Exosc10*$^{C/C}$, *Mb1*$^{cre/+}$ *Dis3*$^{C/+}$, and *Mb1*$^{cre/+}$ *Dis3*$^{C/C}$ mice. (**G**) Quantification of Peyer's patches activated B cells (B220^{+} GL7^{+}). Data were obtained from *Mb1*$^{cre/+}$ *Exosc10*$^{C/+}$, *Mb1*$^{cre/+}$ *Exosc10*$^{C/C}$, *Mb1*$^{cre/+}$ *Dis3*$^{C/+}$, and *Mb1*$^{cre/+}$ *Dis3*$^{C/C}$ mice. These results are representative from at least three independent experiments, using a total of at least three mice per group. Bar graphs show mean value ± SEM, analyzed with two-tailed unpaired *t* test. **P* < 0.05; ***P* < 0.01; ****P* < 0.001.

Noncoding transcription at *Ig* genes during V(D)J recombination (*9*) correlates with chromatin accessibility to the transcription and recombination machineries (*3*, *4*). The processing machinery of *Ig* locus/V(D)J recombination–associated ncRNAs is known; however, direct implication of ncRNAs in V(D)J recombination events has not been evaluated thus far. By focusing our RNA-seq analysis specifically on the *Igh* locus, we observed an increase in antisense germline transcription overlapping J_H (Fig. 4E) and D genes (Fig. 4F), potentially impeding the first step of D to J_H recombination (fig. S3A). Although we observed weak germline noncoding transcription at V_H genes in control cells, we found a substantial accumulation of ncRNAs spread over all the V_H genes in the absence of RNA exosome activity (Fig. 4, G to I). These transcripts were mainly antisense ncRNAs overlapping RSS and V_H genes (Fig. 4, G and H, and fig. S6, A to D) that may interfere with RAG binding, cleavage, and/or accessibility at these recombination sites. We showed an inverse correlation between ncRNA accumulation and decreased coding of V_H expression in the absence of DIS3 (fig. S6E). These data suggest that *Igh* germline transcription is sensitive to DIS3 activity and in the absence of ncRNA processing, V(D)J recombination at *Igh* loci is decreased.

Next, we analyzed differentially expressed genes in pro–B cells (fig. S6F and table S1) and evaluated overall impact of the RNA exosome in pro–B cell biology by performing gene set enrichment analysis. Affected Kyoto Encyclopedia of Genes and Genomes (KEGG) pathways were related to pro–B cell maturation including hematopoietic cell lineage or mitogen-activated protein kinase (MAPK) signaling pathways, for example (Fig. 4J). DIS3-deficient cells have increased expression of p53 pathway–associated genes (Fig. 4J), leading to programmed cell death to avoid the accumulation of pro–B cells harboring unproductive V(D)J recombination (*28*) along with mRNA expression perturbations and/or DNA damage response (*25*). We showed the increased expression of *Trp53* (Fig. 4K) and associated genes from RNA-seq data (Fig. 4L). We performed independent experiments to confirm the increased expression of the p53 pathway–associated genes observed in the RNA-seq data (fig. S6G) by reverse transcription quantitative PCR (qPCR). Increased expression of p53 pathway–associated genes ultimately led to apoptosis in the absence of DIS3 and ncRNA processing (fig. S6H). These observations corroborate the pro–B cell blockade phenotype and pre–B cell differentiation defect in the absence of RNA exosome. V(D)J recombination components themselves (including *Rag* recombinase expression) and related pathways were not affected in DIS3-deficient cells.

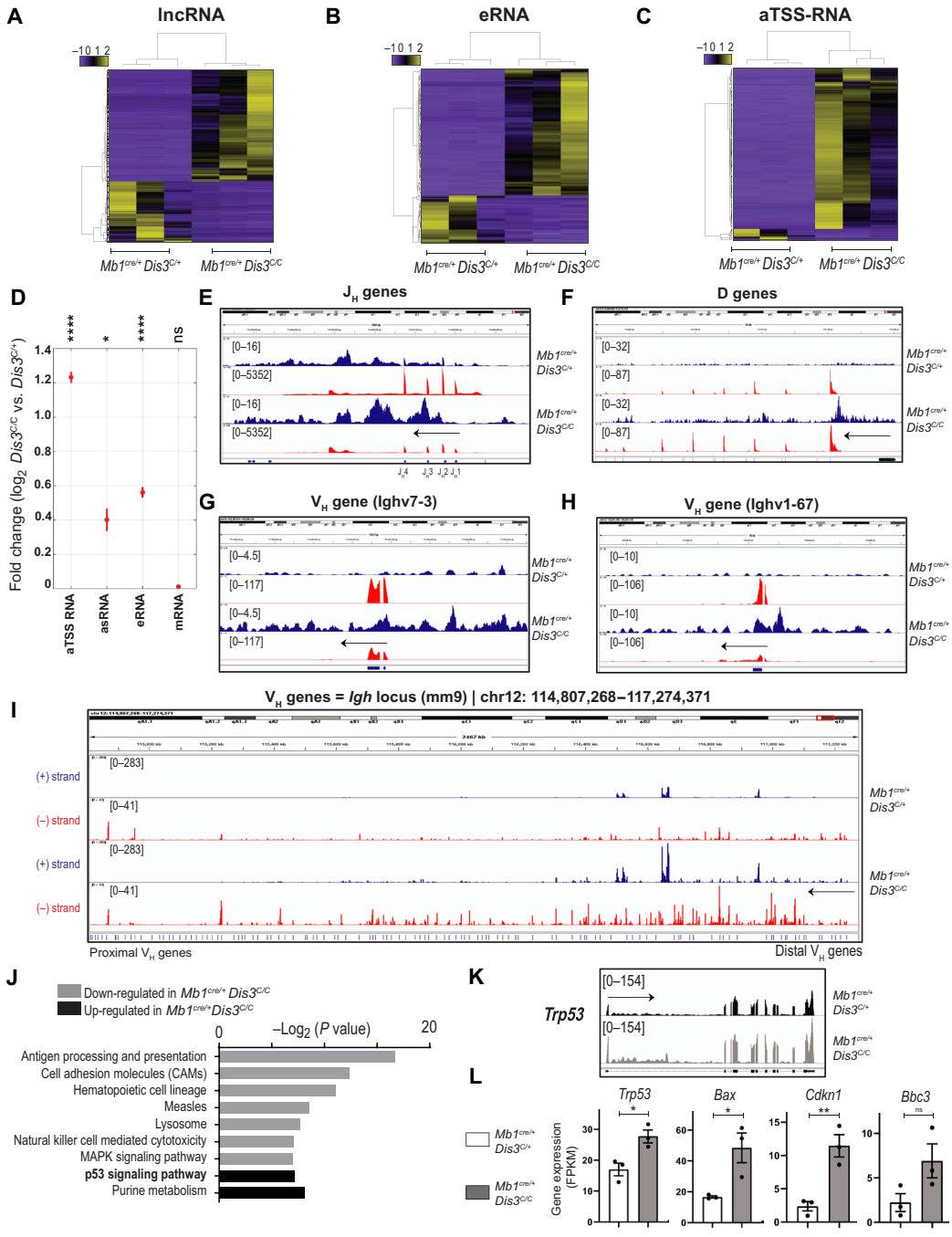

Fig. 4. RNA-seq reveals RNA exosome substrates from pro–B cells in vivo. RNA-seq of pro–B cells from *Mb1*$^{cre/+}$ *Dis3*$^{C/+}$ and *Mb1*$^{cre/+}$ *Dis3*$^{C/C}$ mice. (**A**) Heatmap showing the lncRNAs up-regulated (yellow, 2544) and down-regulated (purple, 1405) in the absence of DIS3. (**B**) Heatmap showing the eRNAs up-regulated (157) and down-regulated (60) in the absence of DIS3. (**C**) Heatmap showing the aTSS-RNAs up-regulated (461) and down-regulated (35) in the absence of DIS3. Unsupervised hierarchical clustering is shown. (**D**) Genome-wide analysis of DIS3-sensitive RNA substrates in pro–B cells in vivo. The fold increase for the different classes of ncRNAs is shown, including aTSS-RNAs, asRNAs, eRNAs, and mRNA, Wilcoxon rank sum test. (**E** to **I**) Three independent RNA-seq experiments were performed showing similar results. The data were combined for a better visualization using the IGV viewer and to present the RNA tracks. Because of strand-specific sequencing, + (blue) tracks represent the RNA corresponding to the Watson DNA strand, – (red) tracks represent the RNA corresponding to the Crick DNA strand, and black arrows indicate the direction of coding transcription. (E) Accumulation of ncRNAs at the J_H1 to J_H4 genes region in the absence of RNA exosome activity. (F) Accumulation of ncRNAs at the D genes region in the absence of RNA exosome activity. (G) Example of ncRNA accumulation at V_H (Ighv7-3) gene in the absence of RNA exosome activity, while coding gene expression is decreased. (H) Example of ncRNA accumulation at V_H (Ighv1-67) gene in the absence of RNA exosome activity, while coding gene expression is decreased. (I) ncRNA accumulation at the *Igh* locus in DIS3-deficient pro–B cells. The *Igh* locus is shown from the first to the last V_H genes. Sense (red) and antisense (blue) ncRNAs are shown in *Mb1*$^{cre/+}$ *Dis3*$^{C/+}$ and *Mb1*$^{cre/+}$ *Dis3*$^{C/C}$ pro–B cells, these tracks represent ncRNAs only, after removal of V_H coding transcripts. (**J**) Gene set enrichment analyses are shown from these lists of differentially expressed genes. The down-regulated (gray) and up-regulated (black) KEGG pathways are shown. (**K**) *Trp53* expression in the absence of DIS3. (**L**) Overexpression of *Trp53* and associated genes in the absence of DIS3 (two-tailed unpaired *t* test). *$P < 0.05$; **$P < 0.01$; ****$P < 0.0001$.

Together, these results suggest that the V(D)J recombination defect in the absence of DIS3 is not caused by abnormal gene expression of V(D)J recombination regulatory pathways, as deregulated pathways in DIS3-deficient B cells were not related to DNA recombination or programmed DNA repair themselves (Fig. 4J). Rather, our data reveal genome-wide accumulation of ncRNAs (Fig. 4D), especially of germline transcripts at the *Ig* loci (Fig. 4, E to I), raising the possibility of a crucial role of the RNA exosome in the regulation of expression of ncRNAs enabling proper V(D)J recombination.

A rearranged *Igh* allele rescues pro–B cell to pre–B cell differentiation

Defects in V(D)J recombination can be rescued using a prearranged T cell receptor/BCR, even in the absence of RAG recombinases (*29*). We introduced a prearranged *Igh* VDJ gene, i.e., $V_HB1\text{-}8$ allele (Fig. 5A and fig. S7A) (*30*) in the $Mb1^{cre}$ $Dis3^{COIN}$ mice to evaluate a potential rescue in B cell development in the absence of RNA exosome activity. We confirmed an efficient deletion of the $Dis3^{COIN}$ alleles in the $V_HB1\text{-}8^{KI/KI}$ $Mb1^{cre/+}$ $Dis3^{COIN}$ B splenocytes. First, we used flow cytometry to directly visualize *Dis3* relative expression. $V_HB1\text{-}8^{KI/KI}$ $Mb1^{cre/+}$ $Dis3^{C+/}$ B cells demonstrated expression of GFP (i.e., *Dis3*), in experiments using $V_HB1\text{-}8^{KI/KI}$ $Mb1^{cre/+}$ $Dis3^{+/+}$ B cells as control (Fig. 5B). $V_HB1\text{-}8^{KI/KI}$ $Mb1^{cre/+}$ $Dis3^{C/C}$ have stronger GFP expression than heterozygous cells, as would be predicted on the basis of two $Dis3^{COIN}$-inverted alleles (Fig. 5B). We sorted B cells, and qPCR quantification confirmed a robust deletion of the $Dis3^{COIN}$ allele, specifically in B cells expressing a *cre* recombinase, with ~50% of deletion in heterozygous cells and ~95% of deletion in homozygous cells (fig. S7B). These data suggest that a fraction of B cells was able to develop efficiently in the absence of DIS3 when they express a knock-in transgenic BCR.

Under these conditions $V_HB1\text{-}8^{KI/KI}$ $Mb1^{cre/+}$ $Dis3^{C/C}$ B cells were able to differentiate to a similar level as $V_HB1\text{-}8^{KI/KI}$ $Mb1^{cre/+}$ $Dis3^{C/+}$ progenitors from the pro–B cell to the small pre–B cell stage (Fig. 5, C and D), suggesting the role of the RNA exosome complex in VDJ recombination and subsequent differentiation into pre–B cells. In this model, V_L to J_L recombination is dependent on endogenous *Igl* genes in pre–B cells. Thus, in the absence of IgL rescue, the subsequent differentiation into immature B cells was reduced in the bone marrow (Fig. 5, C and D), with fewer peripheral B cells observed in the spleen in the absence of DIS3 (fig. S7, C and D). In addition, the MZ/follicular B cell ratio was also higher in this $V_HB1\text{-}8^{KI/KI}$ $Mb1^{cre/+}$ $Dis3^{C/C}$ model (fig. S7E). Collectively, these results directly demonstrated RNA exosome's function in V(D)J recombination specifically during the pro–B cell to pre–B cell transition.

Dis3 deletion leads to decreased recombination in the *Igκ* light chain

Although pro–B cells are differentiating from lymphoid progenitors with *Igh* genes accessible and primed to undergo VDJ recombination, *Igκ* recombination depends on successful recombination and expression of the pre-BCR. To understand whether open chromatin (accessibility) of the *Igκ* locus is widely affected in DIS3-deficient B cells, we performed ATAC-seq assays in sorted pro–B cell populations. Genome-wide analyses reveal a selective impact of DIS3 loss on chromatin accessibility, with more than 6000 peaks decreased in the absence of RNA processing and fewer than 1000 peaks showing increased accessibility (fig. S8, A and B, and table S2). A total of 175 peaks were decreased at CTCF-binding elements (CBEs), whereas

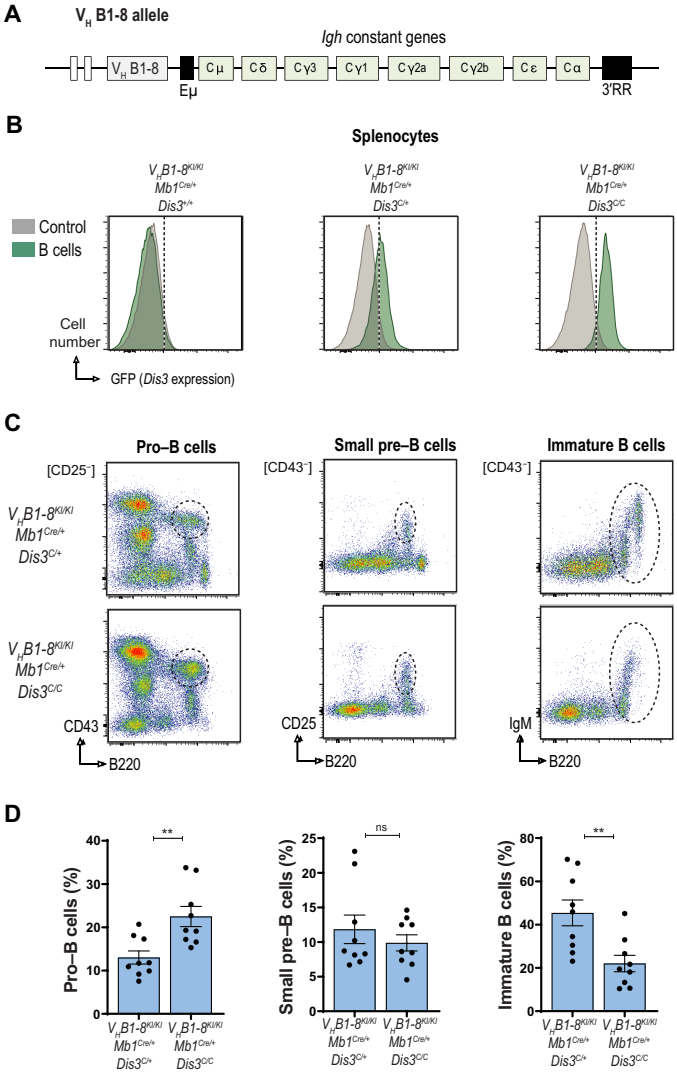

Fig. 5. Introduction of a prearranged VDJ gene restores pre–B cell population. (**A**) Schematic of the $V_HB1\text{-}8$ knock-in ($V_HB1\text{-}8^{KI}$) allele. $Mb1^{cre/+}$ $Dis3^{COIN}$ mice were crossed with $V_HB1\text{-}8^{KI}$ mice to generate the $V_HB1\text{-}8^{KI/KI}$ $Mb1^{cre/+}$ $Dis3^{C/+}$ and $V_HB1\text{-}8^{KI/KI}$ $Mb1^{cre/+}$ $Dis3^{C/C}$ mouse models. (**B**) Representative FACS plots showing the GFP expression (i.e., *Dis3* expression) from $V_HB1\text{-}8^{KI/KI}$ $Mb1^{cre/+}$ $Dis3^{+/+}$, $V_HB1\text{-}8^{KI/KI}$ $Mb1^{cre/+}$ $Dis3^{C/+}$, and $V_HB1\text{-}8^{KI/KI}$ $Mb1^{cre/+}$ $Dis3^{C/C}$ cells. The gray histograms represent GFP expression in control cells ($B220^-$), whereas the green histograms show GFP expression in B cells ($B220^+$ Igk^+). (**C**) Flow cytometry analyses of bone marrow pro–B cells ($CD43^+$, $B220^+$, $CD25^-$, and IgM^-), small pre–B cells ($CD43^-$, $B220^+$, $CD25^+$, and IgM^-) and immature B cells ($CD43^-$, $B220^+$, $CD25^-$, and IgM^+) populations from $V_HB1\text{-}8^{KI/KI}$ $Mb1^{cre/+}$ $Dis3^{C/+}$ and $V_HB1\text{-}8^{KI/KI}$ $Mb1^{cre/+}$ $Dis3^{C/C}$ mice. (**D**) Quantification of bone marrow pro–B, small pre–B, and immature B cell populations from $V_HB1\text{-}8^{KI/KI}$ $Mb1^{cre/+}$ $Dis3^{C/+}$ and $V_HB1\text{-}8^{KI/KI}$ $Mb1^{cre/+}$ $Dis3^{C/C}$ mice. These results are representative from six independent experiments, using a total of nine mice per group. Bar graphs show mean value ± SEM, analyzed with two-tailed unpaired *t* test. $^{**}P < 0.01$.

only 7 were increased; 162 peaks showed less accessibility at promoters, whereas 175 peaks gained accessibility. These differences in accessibility could reflect different maturational stages, with DIS3-proficient cells prone to differentiate, whereas DIS3-deficient cells are blocked at the pro–B cell stage. Last, 606 peaks were decreased at enhancer regions, but no gains were observed at enhancers (fig. S8C). We evaluated DNA accessibility at the *Igκ* alleles in

DIS3-proficient versus DIS3-deficient cells and observed decreased accessibility in some parts of this locus. However, most of *Igκ* still had open chromatin (Fig. 6A). Thus, chromatin accessibility was mostly intact during *Vκ* to *Jκ* gene rearrangements in DIS3-deficient B cells. In contrast, *Vκ* recombination was decreased across the *Igκ* locus in DIS3-deficient B cells (Fig. 6, B and C). Total productive *Igk* rearrangements were decreased from 4566 functional VκJκ junctions of 648,140,008 reads in controls (7.05 per million reads) to 933 functional VκJκ junctions of 671,548,696 reads (1.39 per million reads) in the absence of DIS3, about a factor of 5 (Fig. 6, B and C), but *Igλ* recombination level was affected only from 207 functional VλJλ junctions of 648,140,008 reads in controls (0.32 per million reads) to 98 functional VlJλ junctions of 671,548,696 reads (0.15 per million reads), about a factor of 2 (Fig. 6, D and E), resulting in a higher proportion of *Igλ* recombination (Fig. 6F) in our repertoire analysis. *Vκ* and *Vλ* usages were not skewed (fig. S8, D and E). As previously mentioned, $V_HB1\text{-}8^{KI}$ mice harbor a prearranged V(D)J gene and still have to recombine the Ig light chain to develop immature and mature B cells. We evaluated *Igκ* recombination in these cells by flow cytometry and again found fewer $Igκ^+$ mature B cells in the periphery compared with the control (Fig. 6, G and H). Together, our data revealed a critical contribution of DIS3 to successful recombination of *Igk* genes, whereas *Igλ* was less affected.

DISCUSSION

The RNA exosome complex has critical functions during B cell activation, including (i) critical regulation of ncRNAs overlapping switch sequences, (ii) giving accessibility to both DNA strands for AID-mediated cytidine deamination for efficient CSR (*21*, *22*, *24*), and (iii) controlling chromosomal architecture (*10*). Outside the *Igh* locus, super enhancer–associated RNA exosome–sensitive ncRNA transcription recruits AID activity causing oncogenic mutations (*24*, *25*). In agreement with these important functions, expression profile analyses of RNA exosome complex subunits demonstrated enhanced expression in the GC. We found that RNA exosome subunit

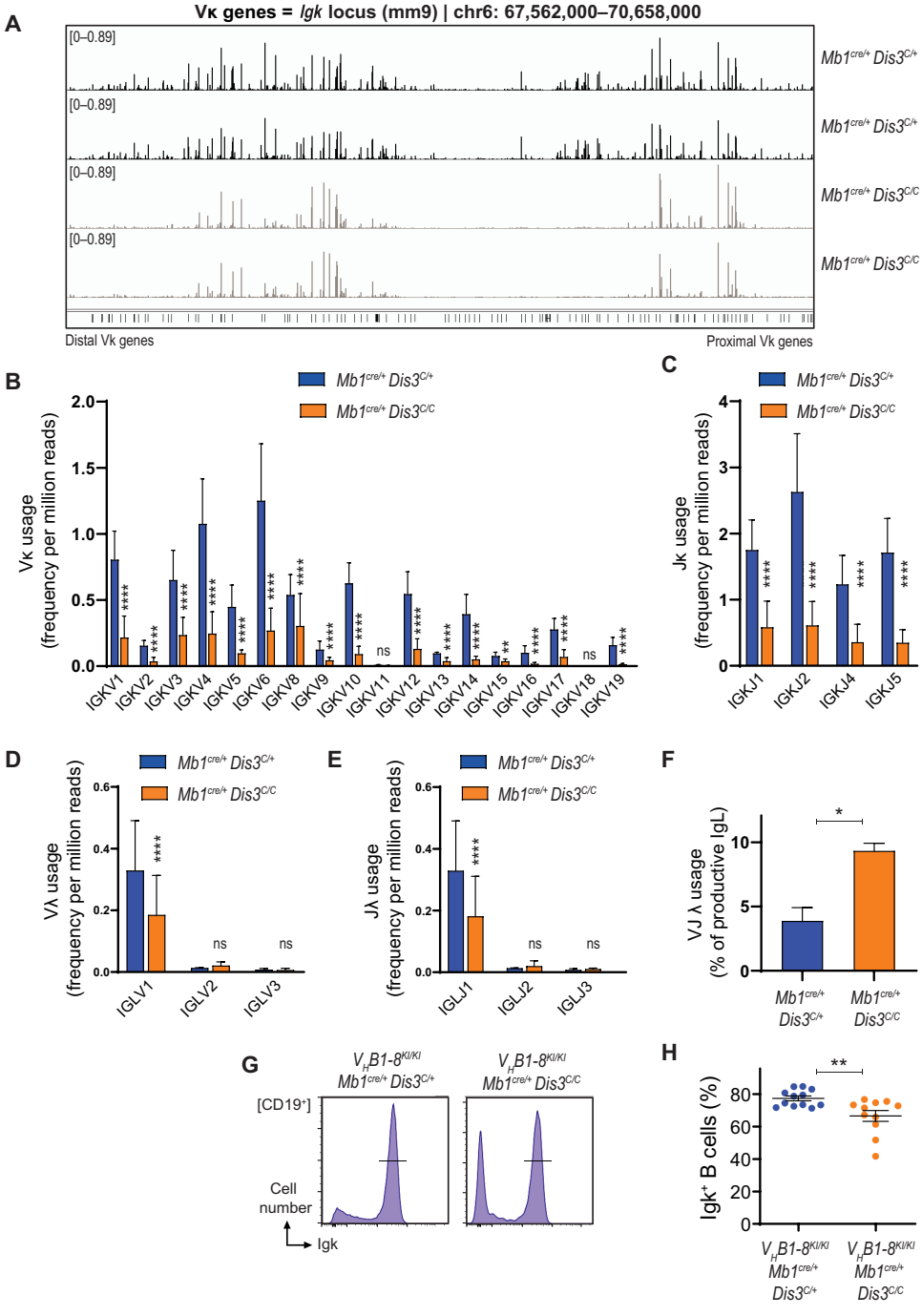

Fig. 6. Chromatin accessibility and *IgL* recombination in the absence of RNA processing. (**A**) ATAC-seq experiments were performed on pro–B cells from $Mb1^{cre/+}$ $Dis3^{C/+}$ and $Mb1^{cre/+}$ $Dis3^{C/C}$ mice, accessibility of *Vκ* genes is shown (two independent experiments). (**B**) *Vκ* repertoire in $Mb1^{cre/+}$ $Dis3^{C/+}$ and $Mb1^{cre/+}$ $Dis3^{C/C}$ pro–B cells. (**C**) *Jk* repertoire in $Mb1^{cre/+}$ $Dis3^{C/+}$ and $Mb1^{cre/+}$ $Dis3^{C/C}$ pro–B cells. (**D**) *Vλ* repertoire in $Mb1^{cre/+}$ $Dis3^{C/+}$ and $Mb1^{cre/+}$ $Dis3^{C/C}$ pro–B cells. (**E**) *Jλ* repertoire in $Mb1^{cre/+}$ $Dis3^{C/+}$ and $Mb1^{cre/+}$ $Dis3^{C/C}$ pro–B cells. The VJ repertoire was determined by RNA-seq of pro–B cells (three independent experiments, mean is shown, ±SEM), and the number of productive VJ rearrangements compared with the total number of reads was used to perform statistical analyses (Khi2 proportion test). (**F**) The number of productive Igλ rearrangements among the total number of productive IgL rearrangements was determined (three independent experiments, two-tailed paired *t* test). (**G**) Flow cytometry analyses of Igk expression on B splenocytes ($CD19^+$) from $V_HB1\text{-}8^{KI/KI}$ $Mb1^{cre/+}$ $Dis3^{C/+}$ and $V_HB1\text{-}8^{KI/KI}$ $Mb1^{cre/+}$ $Dis3^{C/C}$ mice. (**H**) Quantification of Igk expression on B splenocytes ($CD19^+$) from $V_HB1\text{-}8^{KI/KI}$ $Mb1^{cre/+}$ $Dis3^{C/+}$ and $V_HB1\text{-}8^{KI/KI}$ $Mb1^{cre/+}$ $Dis3^{C/C}$ mice. Six independent experiments ($n = 11$ to 12 mice), mean is shown, ±SEM, two-tailed unpaired *t* test. $^*P < 0.05$; $^{**}P < 0.01$; $^{****}P < 0.0001$.

expressions are also increased during V(D)J recombination in bone marrow B cells, piquing our interest in their function in early B cell development. Our observations indicate an evolutionarily designed mechanism to coregulate the expression of the different RNA exosome subunits during two crucial steps of B cell development.

We observed that some of the RNA exosome subunit promoters share common transcription factor binding sites, suggesting their concomitant regulation in B cells, whereas other additional regulatory elements potentially add function in a cell-specific manner. Most of the RNA exosome subunits also have increased expression in B1a B cells in the spleen. B1a B cells are long-lived, self-renewing innate-like B cells and have potential implications in viral clearance (*31*), suggesting that increased expression of the RNA exosome subunits could be implicated in antiviral immunity, potentially by directly degrading viral RNAs (*32*). RNA exosome–deficient mice have a severe defect in B cell development, with B cell accumulation at the pro–B cell stage. Consequently, development of peripheral follicular B cells is strongly affected because RNA exosome–deficient B cells cannot migrate and survive in the periphery. However, we observe normal MZ B cell compartments. These differences in follicular B cells versus MZ B cells could be due to differences in the kinetics of RNA exosome subunit deletion in our mouse model or could be a due to a more mechanistic and biological reason that we do not yet understand.

Tonic BCR signaling controls B cell fate, with low tonic signaling usually favoring MZ differentiation (*2*, *33*). We observed weak expression of the BCR in the absence of the RNA exosome and postulated that this arises because of a suboptimal 3D configuration of the *Igh* locus and accumulation of ncRNAs at the 3′RR and Eμ enhancers, with Eμ controlling heavy chain expression (*34*). Thus, it is possible that weak BCR expression induces low tonic signaling and promotes MZ B cell differentiation in our models. Further investigation will determine how the RNA complex could specifically regulate B cell fate and whether its activity is more dispensable for MZ B cells. We sequenced the noncoding transcriptome from primary pro–B cells in which *Dis3* gene deletion was very efficient in vivo. In activated B cells, lncRNAs, eRNAs, aTSS-RNAs, and asRNAs are DIS3 substrates (*10*). The RNA exosome has the ability to degrade these categories of ncRNAs ubiquitously (independent of the cell type), whereas specific functions are ensured by distinct expression patterns of RNA exosome–sensitive ncRNAs (i.e., germline ncRNAs at V_H genes or germline ncRNAs at switch regions).

A complete understanding of the interplay between RNA processing and chromatin modifications remains elusive, although circumstantial evidence indicates that chromatin-associated RNAs can influence epigenetic and transcriptional outcomes (*17*, *35*–*38*). Chromatin-associated lncRNAs also have been shown to function in CTCF site regulation and local chromosomal architecture (*39*). In developing pro–B cells, we observed a moderate impact of RNA exosome–mediated RNA processing on chromatin accessibility, with both *Igh* and *Igκ* having strong recombination defects but mild effects on ATAC-seq–measured chromatin accessibility in DIS3-deficient cells.

Accessibility at promoter sequences was variable, with gain and loss, possibly because of different differentiation stages. Enhancer-expressed ncRNAs (eRNAs) (*40*) are processed by the RNA exosome (*25*). In the absence of RNA processing, we observed an accumulation of eRNAs along with decreased chromatin accessibility at some enhancers, although almost no gain was seen, suggesting that ncRNA accumulation at enhancers mostly leads to decreased accessibility. The RNA exosome is associated with transcription elongation and termination (*41*, *42*), and chromatin accessibility at enhancers could be perturbed by an alteration of RNA polymerase II configuration at these sites. However, widespread effects on chromatin accessibility may not occur after RNA exosome deficiency or are not observable in our in vivo model systems due to experimental limitations.

We demonstrated that DIS3 regulates germline transcripts, strongly expressed during V(D)J recombination and normally processed by the RNA surveillance machinery. Many factors contribute to and regulate V(D)J recombination including RSS sequences composition, chromatin accessibility, epigenetic chromatin marks, transcription factor binding, chromatin architecture protein occupancy (including cohesin and CTCF), or sense and antisense transcription (*43*, *44*). We propose now that RNA processing of ncRNAs by the RNA exosome and its cofactors is an important additional requirement for optimal V(D)J recombination.

It seems noncoding transcription could be critical for appropriate chromatin structure and nucleosome positioning (*45*) before V(D)J recombination. RNA exosome–deficient cells tend to accumulate chromatin-associated RNAs (*10*, *16*) that may interfere with RAG1/2 DNA binding necessary for catalysis of DNA breaks at RSS sequences. Decreased V(D)J recombination in the absence of DIS3 may explain why V(D)J recombination can occur in the absence of transcription (*46*–*48*), as germline transcription is likely a consequence of accessible chromatin but is not absolutely required for recombination. We propose that germline ncRNAs might be resolved by the RNA processing machinery to complete this process. To reach a definitive conclusion on the impact of RNA exosome deficiency on V(D)J recombination, we rescued the developmental defect at the pro–/pre–B cell transition by introducing a prearranged *Igh* V_HB1-*8* allele. The expression of this transgenic V(D)J allele partly restores normal levels of pre–B cells. Although RNA exosome activity could control many other aspects of the pro–B cell to pre–B cell transition, this rescue experiment suggests a direct implication of the RNA exosome complex in V(D)J recombination. Moreover, alteration of CDR3 length also suggests that ncRNA processing is necessary to generate physiological CDR3 junctions, whereas chromatin-associated ncRNA and/or RNA:DNA hybrids accumulation eventually interferes with the DNA repair machinery (*25*, *49*).

Although cellular proliferation could be affected in the absence of DIS3, it is unlikely to affect RAG-mediated DNA breaks and DNA repair that occur in nonproliferative pro–B cells. RAG scanning during V(D)J recombination is dependent on chromatin loop extrusion mediated by CTCF binding at CBEs in concert with cohesin translocation on the Ig loci (*11*–*13*). DIS3 deficiency leads to an accumulation of chromatin-associated ncRNAs along with disorganized cohesin localization in activated B cells; thus, ncRNA transcription and processing that may generate non–B DNA structures are possible mechanisms for regulating loop extrusion kinetics (*10*). It is possible that a similar mechanism due to aberrant ncRNA accumulation interferes with physiological loop extrusion kinetics during V(D)J recombination and RAG scanning, thereby impeding RAG-mediated DNA cleavage and V(D)J recombination in the absence of the RNA exosome. These possibilities will be experimentally tested in future studies.

Last, we consider the pathological consequence of RNA exosome function deficiency in humans where mutations in the RNA helicase *SKIV2L* (an RNA helicase cofactor of the RNA exosome complex)

have been associated with THES syndrome (*20*), a rare disease characterized by immunodeficiency and very low antibody titers. A mouse model demonstrates that THES2-like phenotypes can be created successfully by specifically deleting *Skiv2l* during early B cell development, using the same $Mb1^{Cre/+}$ mice crossed with *Skiv2l* floxed alleles [shown in the companion manuscript (*50*)]. Patients with THES2 demonstrate inflammatory responses and a lack of antibody production, but the molecular explanation of antibody deprivation is unknown. After *Skiv2l* deletion through specific flox targeting and *cre* expression in pro–B cells, a developmental defect similar to what we report in core RNA exosome knockout mouse models is observed. However, SKIV2L depletion in mature B cells did not cause class switching defects (*50*). SKIV2L activity is primarily important for supporting RNA exosome–mediated cotranslational decay of mRNAs in the cytoplasm (*51*) by extracting mRNA from stalled 80*S* ribosomes (*52*), and this activity has been validated at a structural level (*53*). Moreover, in SKIV2L mutant immature B cells, nuclear ncRNA stabilization was not observed. Thus, SKIV2L action may indirectly promote nuclear exosome localization and function during early B cell development by keeping the cytoplasmic RNA exosome pool active.

In this study, we show that core RNA exosome component loss leads to a developmental defect in immature B cells similar to previous study where we showed its function in mature B cells and CSR (*24*). During CSR, the accompanying RNA helicase is MTR4, a component of the nuclear exosome targeting (NEXT) complex that unwinds RNA/RNA and DNA/RNA hybrids in the nucleus to facilitate *Igh* DNA recombination (*22*, *54*). Thus, the core RNA exosome functions with different RNA helicases and associated complexes during different steps of *Igh* recombination, namely, with the MTR4/NEXT and other nuclear helicases during CSR and indirectly via the superkiller (SKI) complex during early B cell development. Discovery and characterization of RNA exosome–associated specific nuclear helicases and other cofactors during V(D)J recombination will be important steps forward in understanding the role of ncRNA processing during V(D)J recombination.

MATERIALS AND METHODS

Study design

This study aimed to understand the role of ncRNA processing during the early steps of B cell development and the processes of V(D)J recombination. We developed dedicated mouse models to dissect the functions of the RNA exosome complex, allowing genetic deletion in pro–B cells ($Mb1^{cre/+}$) of one core subunit gene (*Exosc3*) or the catalytic subunit genes (*Exosc10* and *Dis3*), and another model ($V_HB1\text{-}8^{KI/KI}$) to rescue the observed developmental blockade at the pro–B cell stage. These mice were analyzed by flow cytometric analyses, and deeper investigation of ncRNA accumulation was performed through RNA-seq, whereas chromatin accessibility was evaluated by ATAC-sequencing.

Mice

$Mb1^{cre/+}$ mice (*26*) were obtained from M. Reth (University of Freiburg). $V_HB1\text{-}8^{high}$ knock-in mice (named in this study as $V_HB1\text{-}8^{KI/KI}$) (*30*) were provided by M. Nussenzweig (Rockefeller University). *Exosc3*, *Exosc10*, and $Dis3^{COIN}$ alleles have been previously described (*10*, *24*, *25*) and are presented in fig. S1 (B to D). We used heterozygous mice as control (e.g., $Dis3^{COIN/+}$, named as $Dis3^{C/+}$) and homozygous mice as conditional knockout (e.g., $Dis3^{COIN/COIN}$, named as $Dis3^{C/C}$).

Eight- to 12-week male and female mice were used for experiments. Mice experiments were approved by the Columbia University Institutional Animal Care and Use Committee (IACUC) and performed following the recommended guide line of Columbia University (protocol number AC-AABP7556).

Flow cytometry and cell sorting

Bone marrow, spleen, and Peyer's patches were collected from the different mice, and red blood cells were removed by hypotonic lysis (ACK buffer) from the bone marrow and spleen, before saturation in fluorescence-activated cell sorting (FACS) buffer with Fc block (clone 2.4G2, BD Biosciences, 553141) for 10 min at room temperature. Then, cells were stained with antibodies for 30 min at 4°C in FACS buffer [phosphate-buffered saline (PBS) with 3% fetal bovine serum (FBS)], washed, and analyzed.

To study B cell development of $Exosc3^{COIN}$, $Dis3^{COIN}$ mice (both expressing GFP after *COIN* alleles inversion), and $V_HB1\text{-}8^{KI/KI}$ mice, we used the following panel of antibodies: anti-B220 BV510 (clone RA3-6B2, BD Biosciences, 557683), anti-CD43 phycoerythrin (PE) (clone S7, BD Biosciences, 553271), anti-CD25 allophycocyanin (APC) (clone PC61, BD Biosciences, 557192), anti-IgM PE-Cy7 (clone R6-60.2, BD Biosciences, 552867), anti-CD21 APC (clone 7E9, BioLegend, 123411), anti-CD23 PE (clone B3B4, BD Biosciences, 553139), anti-GL7 PE (clone GL7, eBioscience, 12-5902-82), anti-Igk V450 (clone 187.1, BD Biosciences, 561354), and anti-CD19 APC (clone 1D3, BioLegend, 115530). Live cells were gated as lymphocytes and single cells; dead cells were stained with 7-aminoactinomycin D or 4′,6-diamidino-2-phenylindole (DAPI) and excluded from the analyses.

For B cell development analyses of $Exosc10^{COIN}$ mice (expressing RFP after *COIN* allele inversion), the same panel of antibodies was used, substituting anti-B220 Alexa Fluor 700 (clone RA3-6B2, BD Biosciences, 557957), anti-CD43 fluorescein isothiocyanate (FITC; clone S7, BD Biosciences, 553270), anti-CD23 FITC (clone B3B4, BD Biosciences, 561772), and anti-GL7 FITC (clone GL7, BD Biosciences, 562080). Live cells were gated as lymphocytes and single cells; dead cells were stained with DAPI and excluded from the analyses. For CD19 cell sorting, we used anti-CD19 PerCP-Cy5.5 (clone 6D5, BioLegend, 115533). Data were acquired on LSR Fortessa, LSR2, or Accuri C6 (BD Biosciences) machines with subsequent analysis using FlowJo software, and cell sorting was performed on Aria II (BD Biosciences).

PCR and qPCR

For DNA extraction, cells were suspended in proteinase K buffer with proteinase K and incubated overnight at 56°C. Genomic DNA was extracted by ethanol precipitation, washed in 70% ethanol, and suspended in 1X Tris-EDTA (TE) TE buffer. Bone marrow cells were used to evaluate the usage of the different V_H family of genes (distal V_HJ558 versus proximal V_H7183) and D to J_H3 recombination.

PCR was performed on 100, 10, and 1 ng of genomic DNA using the following primers: V_HJ558 gcgaagcttargcctgggrcttcagtgaag (forward) and J_H4 aggctctgagatccctagacag (reverse); V_H7183 cggtaccaagaasamcctgtwcctgcaaatgasc (forward) and J_H4 aggctctgagatccctagacag (reverse); and D aggctctgagatccctagacag (forward) and J_H3 gtctagattctcacaagagtccgatagaccctgg (reverse) as previously described (*55*, *56*). As loading control, Cμ primers are tggccatgggctgcctagcccgggactt (forward) and gcctgactgagctcacacaaggagga (reverse).

qPCR was performed on genomic DNA from $CD19^+$- and $CD19^-$-sorted splenocytes. For $Dis3^{COIN}$ allele inversion, the

following primers were used: *Dis3*^{COIN}, caaggaaaccctggactactg (forward) and aatgggtctagcacatgcacatc (reverse); the qPCR signals were normalized using *Myc* primers: *Myc*, agcgcagcatgaattaactgc (forward) and gtatacgtggcagtgagttg (reverse). qPCR was performed on 50 ng of genomic DNA using SYBR Green and Roche LightCycler II apparatus.

RNA extraction, cDNA synthesis, and qPCR

Total RNA was extracted from FACS-sorted pro–B cells from *Mb1*$^{+/+}$ *Dis3*$^{C/C}$ and *Mb1*$^{cre/+}$ *Dis3*$^{C/C}$ mice using the RNeasy Mini Kit (QIAGEN). cDNA was synthetized using Oligo(dT) primers and SuperScript IV Reverse Transcriptase (Thermo Fisher Scientific). qPCR was assembled using Maxima SYBR Green Mix (2X) (Thermo Fisher Scientific) in triplicates. Gene expression levels were normalized by glyceraldehyde-3-phosphate dehydrogenase (GAPDH), and gene expression levels for individual genes are presented as $2^{-\Delta Ct}$, using the following oligonucleotides: Bbc3, gtgaccactggcattcattg (forward) and ctcctccctcttctgagactt (reverse); Cdkn1, ctggtgatctgctgctcttt (forward) and ccctgcatatacattcccttcc (reverse); Bax, ggagatgaactggacagcaata (forward) and gaagttgccatcagcaaacat (reverse); Trp53, aagatccgcgggcgtaa (forward) and catcctttaactctaaggcctcattc (reverse); and GAPDH, acttcaacagcaactcccactcttc (forward) and tccagggtttcttactccttggag (reverse).

RNA sequencing

Bone marrow were collected from mice, red blood cells were removed by hypotonic lysis (ACK buffer), and cells were saturated in FACS buffer (PBS with 3% FBS) with Fc block (clone 2.4G2) for 10 min at 4°C. Then, cells were stained with antibodies for 30 min at 4°C in FACS buffer and washed, and pro–B cells were sorted as B220^{+}, CD43^{+}, CD25^{-}, IgM^{-}, live singlet cells using a BD Aria cell sorter. RNA was extracted using TRIzol (Invitrogen TRIzol Reagent), RNA quality was evaluated by Bioanalyzer (Agilent), and RNA samples were sequenced using the RNA Ribozero 90M 100PE Sequencing Kit (Illumina) at the Columbia University Genome Center.

Chromatin accessibility assay

Bone marrow preparations from two *Mb1*$^{cre/+}$ *Dis3*$^{C/+}$ and *Mb1*$^{cre/+}$ *Dis3*$^{C/C}$ littermate mice were FACS-sorted to isolate the pro–B cell population (B220^{+} CD43^{+} IgM^{-}). An average of 100,000 pro–B cells were isolated from each mouse. Nuclei isolation and transposition was performed as previously described in the Omni-ATAC protocol (*57*). The total of four samples had libraries synthetized using NEBNext High-Fidelity 2X PCR master mix with NextEra transposase adapter primers containing different indexes. Indexed libraries were multiplexed before and pair-ended sequenced using an Illumina NextSeq instrument.

Statistical analysis

Statistical analyses were performed using GraphPad Prism software, including two-tailed *t* tests (paired or unpaired) and two-tailed proportion tests (χ^2); ns indicates nonstatistically significant; *$P < 0.05$; **$P < 0.01$; ***$P < 0.001$; ****$P < 0.0001$.

Bioinformatics analyses

RNA exosome subunits expression

The expression levels of the RNA exosome subunits were extracted from the "ImmGen data browsers microarray" (www.immgen.org), and the values were plotted as heatmaps.

Motif enrichment analysis

Motif enrichment analysis was performed using MEME Suite 5.4.1. Sequence regions 250–base pair upstream of ATG were retrieved for *Dis3* (chr14: 99,099,669 to 99,099,907), *Exosc3* (chr4: 45,320,580 to 45,320,829), and *Exosc10* (chr4: 148,558,216 to 148,558,471) genes. The following settings were used for motif discovery: Motif discovery mode, classic mode; selected site distribution, any number of repetitions; number of motifs, 3.

Data processing

We use Real Time Analysis (RTA) (Illumina) for base calling and bcl2fastq2 (version 2.17) for converting BCL to fastq format, coupled with adaptor trimming. The resulting reads were mapped to mm9 genome of house mouse by hisat2 (version 2.1.0) (*58*) with default parameters. We used StringTie (version 1.3.3b; parameter "--rf") (*59*) for transcript assembly and expression quantification. The read/fragment counts of features were quantified by FeatureCounts, and the differential features were detected by DESeq2 with criterion of fold change ≥ 2 and false discovery rate (FDR) < 0.05. For visualization in Integrative Genomics Viewer (IGV), we merged bam files from replicates by SAMtools and generated normalized and strand-specific bedgraph files using bedtools and properly calculated scaling factors. The bedgraph files were then converted to bigwig by bedGraph2bigWig utility from the University of California, Santa Cruz (UCSC). For RNA-seq, we used depth-1× normalization method that normalized the sequencing depth to 1× coverage. For ATAC-seq, we use RPM (reads per million mapped reads) normalization.

Differential analysis of lncRNA, eRNA, and aTSS-RNA

lncRNAs that do not overlap with protein-coding exons and with length larger than 200 nt were collected. These RNAs were merged across all samples if they overlapped with each other. The merged transcripts were requantified using FeatureCounts (parameter "-s 2 -p") to obtain the fragment counts table. DESeq2 was applied to the fragment counts table to obtain the differentially expressed lncRNAs (fold change ≥ 2 and FDR < 0.05). These lncRNAs were shown in the heatmap of fragments per kilobase million. We collected ncRNAs that overlap with enhancer regions as eRNA. The enhancer regions were defined by H3K27Ac and H3K4me1 markers from public chromatin immunoprecipitation sequencing (GSM2184223 and GSM2184242). The aTSS-RNA expression was quantified as the ncRNA expression in the anti-TSS region (within 2-kb upstream of TSS but in the antisense strand). The differentially expressed eRNAs and aTSS-RNAs were selected with the same strategy as in the situation of the lncRNA and also are shown in the heatmaps.

Pathway enrichment analysis

The up- and down-regulated gene sets were submitted to DAVID (*60*) for KEGG pathway enrichment analysis. The $-\log_{10}(P \text{ value})$ of each significant ($P < 0.05$) pathway is shown in the bar graph.

Immune repertoire reconstruction analysis

TRUST4 (*61*) with parameters "--abnormalUnmapFlag" was used to reconstruct the immune repertoire.

ATAC-seq analysis

Raw sequencing reads were subjected to adapter trimming by Cutadapt (*62*) with parameters "--trim-n -q 5,5 -m 20 -e 0.1". The resulting reads were mapped to the reference genome of mm9 by bowtie2 (*63*) (version 2.2.9) with parameter "-k 4 -X 2000 --local." Duplicate, multimapped reads and reads that mapped to mitochondria were removed. Peak calling was performed using MACS2 (*64*) (parameter "--nomodel --shift -100 --extsize 200 --broad -f BAMPE").

Bigwig files with RPM normalization were generated for visualization via the IGV or UCSC genome browsers. The peaks across all samples were merged and quantified by FeatureCounts to obtain the read count table. DESeq2 was used to identify the differential peaks. ATAC signals around the summit of differential peaks were plotted in white-blue heatmap.

SUPPLEMENTARY MATERIALS

www.science.org/doi/10.1126/sciimmunol.abn2738
Figs. S1 to S8
Tables S1 to S3

View/request a protocol for this paper from *Bio-protocol*.

REFERENCES AND NOTES

1. S. Herzog, M. Reth, H. Jumaa, Regulation of B-cell proliferation and differentiation by pre-B-cell receptor signalling. *Nat. Rev. Immunol.* **9**, 195–205 (2009).
2. J. C. Yam-Puc, L. Zhang, Y. Zhang, K.-M. Toellner, Role of B-cell receptors for B-cell development and antigen-induced differentiation. *F1000Res.* **7**, 429 (2018).
3. D. G. Schatz, Y. Ji, Recombination centres and the orchestration of V(D)J recombination. *Nat. Rev. Immunol.* **11**, 251–263 (2011).
4. R. M. Cobb, K. J. Oestreich, O. A. Osipovich, E. M. Oltz, Accessibility control of V(D)J recombination. *Adv. Immunol.* **91**, 45–109 (2006).
5. M.-S. Kim, M. Lapkouski, W. Yang, M. Gellert, Crystal structure of the V(D)J recombinase RAG1-RAG2. *Nature* **518**, 507–511 (2015).
6. H. Ru, M. G. Chambers, T.-M. Fu, A. B. Tong, M. Liao, H. Wu, Molecular mechanism of V(D)J Recombination from synaptic RAG1-RAG2 complex structures. *Cell* **163**, 1138–1152 (2015).
7. D. J. Bolland, A. L. Wood, C. M. Johnston, S. F. Bunting, G. Morgan, L. Chakalova, P. J. Fraser, A. E. Corcoran, Antisense intergenic transcription in V(D)J recombination. *Nat. Immunol.* **5**, 630–637 (2004).
8. D. J. Bolland, A. L. Wood, R. Afshar, K. Featherstone, E. M. Oltz, A. E. Corcoran, Antisense intergenic transcription precedes Igh D-to-J recombination and is controlled by the intronic enhancer Emu. *Mol. Cell. Biol.* **27**, 5523–5533 (2007).
9. G. D. Yancopoulos, F. W. Alt, Developmentally controlled and tissue-specific expression of unrearranged VH gene segments. *Cell* **40**, 271–281 (1985).
10. B. Laffleur, J. Lim, W. Zhang, Y. Chen, E. Pefanis, J. Bizarro, C. R. Batista, L. Wu, A. N. Economides, J. Wang, U. Basu, Noncoding RNA processing by DIS3 regulates chromosomal architecture and somatic hypermutation in B cells. *Nat. Genet.* **53**, 230–242 (2021).
11. H.-Q. Dai, H. Hu, J. Lou, A. Y. Ye, Z. Ba, X. Zhang, Y. Zhang, L. Zhao, H. S. Yoon, A. M. Chapdelaine-Williams, N. Kyritsis, H. Chen, K. Johnson, S. Lin, A. Conte, R. Casellas, C.-S. Lee, F. W. Alt, Loop extrusion mediates physiological Igh locus contraction for RAG scanning. *Nature* **590**, 338–343 (2021).
12. Y. Zhang, X. Zhang, Z. Ba, Z. Liang, E. W. Dring, H. Hu, J. Lou, N. Kyritsis, J. Zurita, M. S. Shamim, A. Presser Aiden, E. Lieberman Aiden, F. W. Alt, The fundamental role of chromatin loop extrusion in physiological V(D)J recombination. *Nature* **573**, 600–604 (2019).
13. L. Hill, A. Ebert, M. Jaritz, G. Wutz, K. Nagasaka, H. Tagoh, D. Kostanova-Poliakova, K. Schindler, Q. Sun, P. Bönelt, M. Fischer, J.-M. Peters, M. Busslinger, Wapl repression by Pax5 promotes V gene recombination by Igh loop extrusion. *Nature* **584**, 142–147 (2020).
14. R. M. Brecht, C. C. Liu, H. A. Beilinson, A. Khitun, S. A. Slavoff, D. G. Schatz, Nucleolar localization of RAG1 modulates V(D)J recombination activity. *Proc. Natl. Acad. Sci.* **117**, 4300–4309 (2020).
15. C. Kilchert, S. Wittmann, L. Vasiljeva, The regulation and functions of the nuclear RNA exosome complex. *Nat. Rev. Mol. Cell Biol.* **17**, 227–239 (2016).
16. L. Nair, H. Chung, U. Basu, Regulation of long non-coding RNAs and genome dynamics by the RNA surveillance machinery. *Nat. Rev. Mol. Cell Biol.* **21**, 123–136 (2020).
17. J. Liu, X. Dou, C. Chen, C. Chen, C. Liu, M. M. Xu, S. Zhao, B. Shen, Y. Gao, D. Han, C. He, N6-methyladenosine of chromosome-associated regulatory RNA regulates chromatin state and transcription. *Science* **367**, 580–586 (2020).
18. M. A. Chapman, M. S. Lawrence, J. J. Keats, K. Cibulskis, C. Sougnez, A. C. Schinzel, C. L. Harview, J.-P. Brunet, G. J. Ahmann, M. Adli, K. C. Anderson, K. G. Ardlie, D. Auclair, A. Baker, P. L. Bergsagel, B. E. Bernstein, Y. Drier, R. Fonseca, S. B. Gabriel, C. C. Hofmeister, S. Jagannath, A. J. Jakubowiak, A. Krishnan, J. Levy, T. Liefeld, S. Lonial, S. Mahan, B. Mfuko, S. Monti, L. M. Perkins, R. Onofrio, T. J. Pugh, S. V. Rajkumar, A. H. Ramos, D. S. Siegel, A. Sivachenko, A. K. Stewart, S. Trudel, R. Vij, D. Voet, W. Winckler, T. Zimmerman, J. Carpten, J. Trent, W. C. Hahn, L. A. Garraway, M. Meyerson, E. S. Lander, G. Getz, T. R. Golub, Initial genome sequencing and analysis of multiple myeloma. *Nature* **471**, 467–472 (2011).
19. B. A. Walker, K. Mavrommatis, C. P. Wardell, T. C. Ashby, M. Bauer, F. E. Davies, A. Rosenthal, H. Wang, P. Qu, A. Hoering, M. Samur, F. Towfic, M. Ortiz, E. Flynt, Z. Yu, Z. Yang, D. Rozelle, J. Obenauer, M. Trotter, D. Auclair, J. Keats, N. Bolli, M. Fulciniti, R. Szalat, P. Moreau, B. Durie, A. K. Stewart, H. Goldschmidt, M. S. Raab, H. Einsele, P. Sonneveld, J. S. Miguel, S. Lonial, G. H. Jackson, K. C. Anderson, H. Avet-Loiseau, N. Munshi, A. Thakurta, G. J. Morgan, Identification of novel mutational drivers reveals oncogene dependencies in multiple myeloma. *Blood* **132**, 587–597 (2018).
20. A. Fabre, B. Charroux, C. Martinez-Vinson, B. Roquelaure, E. Odul, E. Sayar, H. Smith, V. Colomb, N. Andre, J.-P. Hugot, O. Goulet, C. Lacoste, J. Sarles, J. Royet, N. Levy, C. Badens, SKIV2L mutations cause syndromic diarrhea, or trichohepatoenteric syndrome. *Am. J. Hum. Genet.* **90**, 689–692 (2012).
21. U. Basu, F.-L. Meng, C. Keim, V. Grinstein, E. Pefanis, J. Eccleston, T. Zhang, D. Myers, C. R. Wasserman, D. R. Wesemann, K. Januszyk, R. I. Gregory, H. Deng, C. D. Lima, F. W. Alt, The RNA exosome targets the AID cytidine deaminase to both strands of transcribed duplex DNA substrates. *Cell* **144**, 353–363 (2011).
22. J. Lim, P. K. Giri, D. Kazadi, B. Laffleur, W. Zhang, V. Grinstein, E. Pefanis, L. M. Brown, E. Ladewig, O. Martin, Y. Chen, R. Rabadan, F. Boyer, G. Rothschild, M. Cogné, E. Pinaud, H. Deng, U. Basu, Nuclear proximity of Mtr4 to RNA exosome restricts DNA mutational asymmetry. *Cell* **169**, 523–537.e15 (2017).
23. S. P. Methot, J. M. Di Noia, Molecular mechanisms of somatic hypermutation and class switch recombination. *Adv. Immunol.* **133**, 37–87 (2017).
24. E. Pefanis, J. Wang, G. Rothschild, J. Lim, J. Chao, R. Rabadan, A. N. Economides, U. Basu, Noncoding RNA transcription targets AID to divergently transcribed loci in B cells. *Nature* **514**, 389–393 (2014).
25. E. Pefanis, J. Wang, G. Rothschild, J. Lim, D. Kazadi, J. Sun, A. Federation, J. Chao, O. Elliott, Z.-P. Liu, A. N. Economides, J. E. Bradner, R. Rabadan, U. Basu, RNA exosome-regulated long non-coding RNA transcription controls super-enhancer activity. *Cell* **161**, 774–789 (2015).
26. E. Hobeika, S. Thiemann, B. Storch, H. Jumaa, P. J. Nielsen, R. Pelanda, M. Reth, Testing gene function early in the B cell lineage in mb1-cre mice. *Proc. Natl. Acad. Sci. U.S.A.* **103**, 13789–13794 (2006).
27. I. Singh, A. Contreras, J. Cordero, K. Rubio, S. Dobersch, S. Günther, S. Jeratsch, A. Mehta, M. Krüger, J. Graumann, W. Seeger, G. Dobreva, T. Braun, G. Barreto, MiCEE is a ncRNA-protein complex that mediates epigenetic silencing and nucleolar organization. *Nat. Genet.* **50**, 990–1001 (2018).
28. C. J. Guidos, C. J. Williams, I. Grandal, G. Knowles, M. T. Huang, J. S. Danska, V(D)J recombination activates a p53-dependent DNA damage checkpoint in scid lymphocyte precursors. *Genes Dev.* **10**, 2038–2054 (1996).
29. Y. Shinkai, S. Koyasu, K. Nakayama, K. M. Murphy, D. Y. Loh, E. L. Reinherz, F. W. Alt, Restoration of T cell development in RAG-2-deficient mice by functional TCR transgenes. *Science* **259**, 822–825 (1993).
30. T.-A. Y. Shih, M. Roederer, M. C. Nussenzweig, Role of antigen receptor affinity in T cell-independent antibody responses in vivo. *Nat. Immunol.* **3**, 399–406 (2002).
31. Y. S. Choi, N. Baumgarth, Dual role for B-1a cells in immunity to influenza virus infection. *J. Exp. Med.* **205**, 3053–3064 (2008).
32. J. M. Molleston, L. R. Sabin, R. H. Moy, S. V. Menghani, K. Rausch, B. Gordesky-Gold, K. C. Hopkins, R. Zhou, T. H. Jensen, J. E. Wilusz, S. Cherry, A conserved virus-induced cytoplasmic TRAMP-like complex recruits the exosome to target viral RNA for degradation. *Genes Dev.* **30**, 1658–1670 (2016).
33. H. Niiro, E. A. Clark, Regulation of B-cell fate by antigen-receptor signals. *Nat. Rev. Immunol.* **2**, 945–956 (2002).
34. M. Marquet, A. Garot, S. Bender, C. Carrion, P. Rouaud, S. Lecardeur, Y. Denizot, M. Cogné, E. Pinaud, The Eμ enhancer region influences H chain expression and B cell fate without impacting IgVH repertoire and immune response in vivo. *J. Immunol.* **193**, 1171–1183 (2014).
35. K. Sarma, C. Cifuentes-Rojas, A. Ergun, A. del Rosario, Y. Jeon, F. White, R. Sadreyev, J. T. Lee, ATRX directs binding of PRC2 to Xist RNA and polycomb targets. *Cell* **159**, 869–883 (2014).
36. J. Sun, C. D. Keim, J. Wang, D. Kazadi, P. M. Oliver, R. Rabadan, U. Basu, E3-ubiquitin ligase Nedd4 determines the fate of AID-associated RNA polymerase II in B cells. *Genes Dev.* **27**, 1821–1833 (2013).
37. X. Wang, R. D. Paucek, A. R. Gooding, Z. Z. Brown, E. J. Ge, T. W. Muir, T. R. Cech, Molecular analysis of PRC2 recruitment to DNA in chromatin and its inhibition by RNA. *Nat. Struct. Mol. Biol.* **24**, 1028–1038 (2017).
38. F. Yang, B. Tanasa, R. Micheletti, K. A. Ohgi, A. K. Aggarwal, M. G. Rosenfeld, Shape of promoter antisense RNAs regulates ligand-induced transcription activation. *Nature* **595**, 444–449 (2021).
39. G. Rothschild, W. Zhang, J. Lim, P. K. Giri, B. Laffleur, Y. Chen, M. Fang, Y. Chen, L. Nair, Z.-P. Liu, H. Deng, L. Hammarström, J. Wang, U. Basu, Noncoding RNA transcription alters chromosomal topology to promote isotype-specific class switch recombination. *Sci. Immunol.* **5**, eaay5864 (2020).

40. T.-K. Kim, M. Hemberg, J. M. Gray, A. M. Costa, D. M. Bear, J. Wu, D. A. Harmin, M. Laptewicz, K. Barbara-Haley, S. Kuersten, E. Markenscoff-Papadimitriou, D. Kuhl, H. Bito, P. F. Worley, G. Kreiman, M. E. Greenberg, Widespread transcription at neuronal activity-regulated enhancers. *Nature* **465**, 182–187 (2010).
41. E. D. Andrulis, J. Werner, A. Nazarian, H. Erdjument-Bromage, P. Tempst, J. T. Lis, The RNA processing exosome is linked to elongating RNA polymerase II in Drosophila. *Nature* **420**, 837–841 (2002).
42. J.-F. Lemay, M. Larochelle, S. Marguerat, S. Atkinson, J. Bähler, F. Bachand, The RNA exosome promotes transcription termination of backtracked RNA polymerase II. *Nat. Struct. Mol. Biol.* **21**, 919–926 (2014).
43. D. J. Bolland, H. Koohy, A. L. Wood, L. S. Matheson, F. Krueger, M. J. T. Stubbington, A. Baizan-Edge, P. Chovanec, B. A. Stubbs, K. Tabbada, S. R. Andrews, M. Spivakov, A. E. Corcoran, Two mutually exclusive local chromatin states drive efficient V(D)J recombination. *Cell Rep.* **15**, 2475–2487 (2016).
44. L. S. Matheson, D. J. Bolland, P. Chovanec, F. Krueger, S. Andrews, H. Koohy, A. E. Corcoran, Local chromatin features including PU.1 and IKAROS binding and H_3K_4 methylation shape the repertoire of immunoglobulin kappa genes chosen for V(D)J recombination. *Front. Immunol.* **8**, 1550 (2017).
45. S. R. Pulivarthy, M. Lion, G. Kuzu, A. G. W. Matthews, M. L. Borowsky, J. Morris, R. E. Kingston, J. H. Dennis, M. Y. Tolstorukov, M. A. Oettinger, Regulated large-scale nucleosome density patterns and precise nucleosome positioning correlate with V(D)J recombination. *Proc. Natl. Acad. Sci. U.S.A.* **113**, E6427–E6436 (2016).
46. C. Angelin-Duclos, K. Calame, Evidence that immunoglobulin VH-DJ recombination does not require germ line transcription of the recombining variable gene segment. *Mol. Cell. Biol.* **18**, 6253–6264 (1998).
47. H. Du, H. Ishii, M. J. Pazin, R. Sen, Activation of 12/23-RSS-dependent RAG cleavage by hSWI/SNF complex in the absence of transcription. *Mol. Cell* **31**, 641–649 (2008).
48. C. Oudinet, F.-Z. Braikia, A. Dauba, A. A. Khamlichi, Recombination may occur in the absence of transcription in the immunoglobulin heavy chain recombination centre. *Nucleic Acids Res.* **48**, 3553–3566 (2020).
49. J. Domingo-Prim, M. Endara-Coll, F. Bonath, S. Jimeno, R. Prados-Carvajal, M. R. Friedländer, P. Huertas, N. Visa, EXOSC10 is required for RPA assembly and controlled DNA end resection at DNA double-strand breaks. *Nat. Commun.* **10**, 2135 (2019).
50. K. Yang, J. Han, J. Gill, J. Park, M. N. Sathe, J. Gattineni, T. Wright, C. Wysocki, T. de la Morena, N. Yan, Trichohepatoenteric syndrome-associated mutation in SKIV2L blocks early B cell development. *Sci. Immunol.* **7**, abn2888 (2022).
51. A. C. Tuck, A. Rankova, A. B. Arpat, L. A. Liechti, D. Hess, V. Iesmantavicius, V. Castelo-Szekely, D. Gatfield, M. Bühler, Mammalian RNA decay pathways are highly specialized and widely linked to translation. *Mol. Cell* **77**, 1222–1236.e13 (2020).
52. A. Zinoviev, R. K. Ayupov, I. S. Abaeva, C. U. T. Hellen, T. V. Pestova, Extraction of mRNA from stalled ribosomes by the Ski complex. *Mol. Cell* **77**, 1340–1349.e6 (2020).
53. A. Kögel, A. Keidel, F. Bonneau, I. B. Schäfer, E. Conti, The human SKI complex regulates channeling of ribosome-bound RNA to the exosome via an intrinsic gatekeeping mechanism. *Mol. Cell* **82**, 756–769.e8 (2022).
54. M. R. Puno, C. D. Lima, Structural basis for MTR4–ZCCHC8 interactions that stimulate the MTR4 helicase in the nuclear exosome-targeting complex. *Proc. Natl. Acad. Sci. U.S.A.* **115**, E5506–E5515 (2018).
55. M. Fuxa, J. Skok, A. Souabni, G. Salvagiotto, E. Roldan, M. Busslinger, Pax5 induces V-to-DJ rearrangements and locus contraction of the immunoglobulin heavy-chain gene. *Genes Dev.* **18**, 411–422 (2004).
56. P. Rouaud, C. Vincent-Fabert, A. Saintamand, R. Fiancette, M. Marquet, I. Robert, B. Reina-San-Martin, E. Pinaud, M. Cogné, Y. Denizot, The IgH 3′ regulatory region controls somatic hypermutation in germinal center B cells. *J. Exp. Med.* **210**, 1501–1507 (2013).
57. M. R. Corces, A. E. Trevino, E. G. Hamilton, P. G. Greenside, N. A. Sinnott-Armstrong, S. Vesuna, A. T. Satpathy, A. J. Rubin, K. S. Montine, B. Wu, A. Kathiria, S. W. Cho, M. R. Mumbach, A. C. Carter, M. Kasowski, L. A. Orloff, V. I. Risca, A. Kundaje, P. A. Khavari, T. J. Montine, W. J. Greenleaf, H. Y. Chang, An improved ATAC-seq protocol reduces background and enables interrogation of frozen tissues. *Nat. Methods* **14**, 959–962 (2017).
58. D. Kim, B. Langmead, S. L. Salzberg, HISAT: A fast spliced aligner with low memory requirements. *Nat. Methods* **12**, 357–360 (2015).
59. M. Pertea, G. M. Pertea, C. M. Antonescu, T.-C. Chang, J. T. Mendell, S. L. Salzberg, StringTie enables improved reconstruction of a transcriptome from RNA-seq reads. *Nat. Biotechnol.* **33**, 290–295 (2015).
60. D. W. Huang, B. T. Sherman, R. A. Lempicki, Systematic and integrative analysis of large gene lists using DAVID bioinformatics resources. *Nat. Protoc.* **4**, 44–57 (2009).
61. L. Song, D. Cohen, Z. Ouyang, Y. Cao, X. Hu, X. S. Liu, TRUST4: Immune repertoire reconstruction from bulk and single-cell RNA-seq data. *Nat. Methods* **18**, 627–630 (2021).
62. M. Martin, Cutadapt removes adapter sequences from high-throughput sequencing reads. *EMBnet. J.* **17**, 10–12 (2011).
63. B. Langmead, S. L. Salzberg, Fast gapped-read alignment with Bowtie 2. *Nat. Methods* **9**, 357–359 (2012).
64. Y. Zhang, T. Liu, C. A. Meyer, J. Eeckhoute, D. S. Johnson, B. E. Bernstein, C. Nusbaum, R. M. Myers, M. Brown, W. Li, X. S. Liu, Model-based analysis of ChIP-seq (MACS). *Genome Biol.* **9**, R137 (2008).

Acknowledgments: We thank M. Nussenzweig (Rockefeller University) for providing *V_HB1-8* mice, M. Reth (University of Freiburg) for *$Mb1^{cre}$* mice, and members of the Basu laboratory and numerous colleagues for very important scientific input. We thank the Columbia University Flow Cytometry Core of the Stem Cell Initiative and Department of Microbiology and Immunology cell sorting facility (both for FACS and cell sorting) and the Columbia University Genome Center (for high-throughput genomics). **Funding:** Research in the Basu laboratory is supported by grants: B.L. (EMBO fellowship, ALTF 906-2015) and U.B. (1R01AI099195, 1RO1 AI143897-01A1, and R01AI134988), Leukemia & Lymphoma Society, and the Pershing Square Sohn Cancer Research Alliance. **Author contributions:** B.L., C.R.B., and U.B. designed and interpreted the experiments, with critical input from J.L. B.L., C.R.B., and B.Y. performed the experiments. W.Z., B.L., D.R., and C.R.B. analyzed the bioinformatics data. L.W., J.E., G.R., J.L., and E.P. helped to develop mouse models. B.L., C.R.B., and U.B. wrote the manuscript. **Competing interests:** The authors declare that they have no competing interests. **Data and materials availability:** All raw sequencing data can be obtained from NIH bioproject with the accession number PRJNA774248. The processed data (bigwig and/or broadpeak) of RNA-seq and ATAC-seq can be obtained from http://52.20.87.23/public/VDJ_project/. Codes related to the analysis are available in https://github.com/basulab-cu/VDJ_project. We also reused these codes https://github.com/basulab-cu. The mouse models used in this study to conditionally delete subunits of RNA exosome can be obtained after completion of a Biological Material Transfer Agreement with Columbia University and Regeneron Pharmaceuticals. All data needed to evaluate the conclusions in the paper are present in the paper or the Supplementary Materials.

Submitted 16 November 2021
Accepted 29 April 2022
Published 3 June 2022
10.1126/sciimmunol.abn2738

Science Immunology

RNA exosome drives early B cell development via noncoding RNA processing mechanisms

Brice LaffleurCarolina R. BatistaWanwei ZhangJunghyun LimBiao YangDelphine RossilleLijing WuJerson EstrellaGerson RothschildEvangelos PefanisUttiya Basu

Sci. Immunol., 7 (72), eabn2738. • DOI: 10.1126/sciimmunol.abn2738

B cells do not Dis3 RNA exosomes

RNA exosomes are complexes that degrade RNA and are involved in cell development. How RNA exosomes affect B cell development is unclear. Here, Laffleur *et al.* found that the expression of various RNA exosome machinery components (Exosc10, Dis3, and Exosc3) were increased at the pro– and pre–B cell phase of B cell development. They made B cell conditional knockout mice for these RNA exosome components and found that these knockouts each led to arrested B cell development at the pro–B cell stage, which correlated to p53-induced cell death and lack of V(D)J recombination. Reintroducing recombination into the Dis3 knockout mice partially rescued this arrest. Thus, the RNA exosome is crucial for B cell development.